Philip de Haes

23 November 2020

Steerable and Reusable Bipolar Vessel Sealer

Design, Development and Validation

Paper

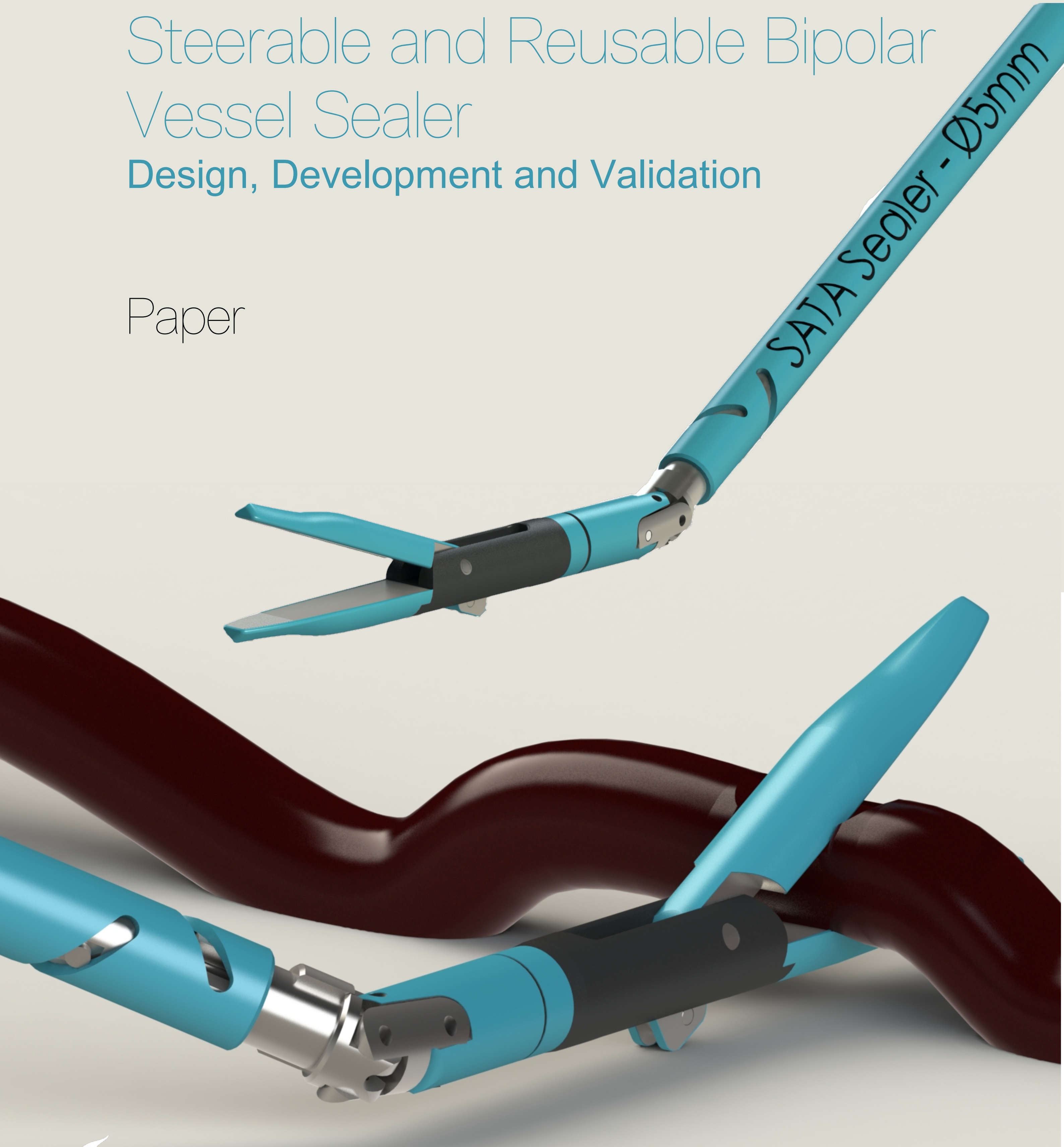

TU Delft

A novel Steerable and Reusable Bipolar Vessel Sealing device designed for developing regions and sustainable healthcare;

Philip de Haes

***Abstract* — A new radical design approach arose from the need to develop a bipolar electrosurgical instrument that is modular and cleanable, thus reusable and therefore suitable for low- and middle-income countries (LMICs). Advanced Bipolar Vessel Sealer (BVS) instruments that are currently on the market cannot be cleaned or maintained well and are therefore most often sold as disposables. Especially in LMICs it is a significant financial burden for hospitals. This possibly leads to the re-use of single-use intended instruments which in turn jeopardizes patient safety. Simultaneously, designing a reusable instrument fits well in the transition to a more circular and sustainable society. To perform advanced laparoscopic surgery with cleanable and affordable electrosurgical instruments, a new design approach is needed. A first phase was initiated by the creation of a cable less steering principle called Shaft Actuated Tip Articulation (SATA) mechanism [1]. Unfortunately, by adding electrically conductive wires to a SATA instrument it loses its modularity and thus cleanability, precisely for which the SATA technology offered a solution in the first place. In addition, there are no non-robotically controlled and reusable BVS instruments with two DOFs available on the market. By being steerable, the user of the instrument is able to deliver a higher quality seal as well as to seal more difficult-to-reach blood vessels and tissue.**

In this thesis project the goal is to redesign a SATA instrument which sustains bipolar vessel sealing and thus designing a BVS that is easy to clean, easily disinfected and sterilized and which is reusable for a vast amount of surgical procedures.

Ideas have been gained by analysing the SATA mechanism and studying commonly used BVS devices. A systematic selection procedure based on the design requirements has resulted in a winning concept for the conduction of electricity through the SATA instrument. For the design of the tip, determining factors were elaborated on, including the construction of the open- and close mechanism and the force transmission ratio between the required seal force on the blood vessel or tissue and the necessary tensile force in the core of the instrument.

The most critical components of the final model have been identified and evaluated by means of FEM simulations and an experiment. The FEM simulations of the tip components show that the design is satisfactory and that a safety factor of ~1.5 has been achieved. This means that these components do not fail due to normal use and they have a long lifespan as well. In the experiment a flexible nitinol guidewire with Teflon coating was tested for wear by pulling the guidewire through an angled SATA hinge. After some necessary adjustments and additions to the design of the BVS, the results were improved but not optimal.

The outcome of this project is a good basis for the BVS design where the steerability has been maintained as well as the modularity and cleanability. The reusability depending on the flexible coating around the core needs to be further investigated and improved.

***Keywords* —** Minimally invasive surgery; laparoscopic instrument; bipolar vessel sealer; steerable; reusable; LMIC; sustainable healthcare; design

Introduction

The need for designing a new BVS arises from the use of laparoscopic instruments in developing areas, where the use of disposable instruments is often not financially feasible and simultaneously the possibilities for cleaning and sterilizing instruments are limited.

Particularly in developed countries, many surgical procedures are preferably performed through minimally invasive surgery (MIS). Decreased blood loss, reduced risk of infection, less postoperative pain and shorter hospital stay are some known advantages of MIS over open surgery [2-5]. The benefits of MIS over open surgery are perhaps even more important in low- and middle-income countries (LMICs), where access to clean water and sanitary living conditions are much more limited and blood banks are scarce [6]. There are however significant barriers to the uptake of MIS in LMICs, high cost of equipment and instruments, difficult sterilisation procedures and lack of training are examples of such challenges.

Over the years a wide variety of laparoscopic instruments have been designed to be used during MIS. While some instruments are reusable, often laparoscopic instruments are intended for single use and should therefore be disposed after each procedure to avoid complex sterilisation and ensure patient safety [7].

One essential instrument that is used during MIS is a Bipolar Vessel Sealer (BVS). This laparoscopic device uses a lower intensity radio-frequency (RF) bipolar current together with an accurate tissue clamping force to seal blood vessels and other tissues. In bipolar configuration both jaws in the tip of the instrument are part of the electrodes, one active and one return. Figure 1 shows an example of a BVS.

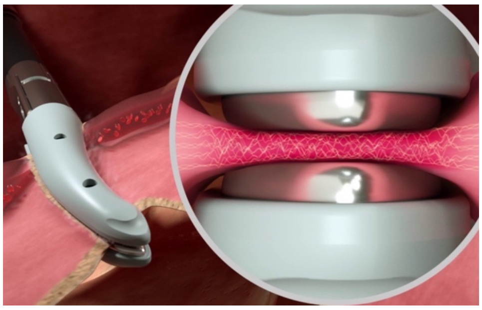

Figure 1, Animation of a vessel being clamped between the jaws of a LigaSure Bipolar Vessel Sealer. © Covidien [8].

Furthermore, designing a reusable BVS fits well in the transition to a more circular society. The global healthcare sector is rapidly growing due to ageing populations, population expansion and new developing markets [9]. Therefore, the use of medical instruments is increasing and more and more waste is being created. On average, the amount of waste created per (hospital) patient each day in the US is 8.4 kg [10]. In European countries, such as France (3.3 kg) and Germany (3.6 kg), less than half of the US waste is created. Mass consumption and an exponential growth in the use of disposables have a negative effect on the costs and availability of raw materials. This causes a growing demand in circularity for sustainable surgery and a sustainable healthcare industry.

Shaft Actuated Tip Articulation (SATA): A steerable vessel sealer offers more reachability to harder to reach tissues, better tissue alignment and reduces the need for using grasping and manipulation tools. This enables the surgeon to seal vessels and tissues easier and more precise which improves the seal quality.

With the introduction of Shaft Actuated Tip Articulation (SATA) technology [1], a cableless, steerable laparoscopic grasping instrument is already designed. Simultaneously, SATA fulfils the need of being modular and cleanable, see Figure 2. By being cableless and modular, SATA instruments are easily assembled and disassembled to allow thorough cleaning and sterilisation. At the same time, low-tech cleaning methods are sufficient for this process [1]. SATA offers two DOFs namely; left and right 'yaw' motion and 'roll' motion along its longitudinal axis as shown in Figure 2. In comparison, current non-robotic bipolar vessel sealers often do not have more than one DOF in tip movement (steerable) and instruments that do have more than one DOF are intended for single use, i.e. not reusable.

Because of the features that SATA instruments offer, it was decided to implement this technology in the design of a steerable and reusable BVS. In the new design, the SATA instrument will form the basis. However, current SATA technology is not directly compatible with electrosurgical instruments because the addition of electrical wires will affect the modularity and steerability. For this reason, an alternative must be found to replace conventional electrical wires and to conduct electricity using the various modular components of the instrument.

Prior to the design project, a literature research into conductive and insulative coatings was conducted to identify coatings that could possibly be used and implemented into the design of a SATA instrument [11]. The use of strategically applied ceramic insulative coatings can be a solution for replacing conventional electrical wires, allowing the SATA instrument to maintain its modularity and thus cleanability and reusability [11].

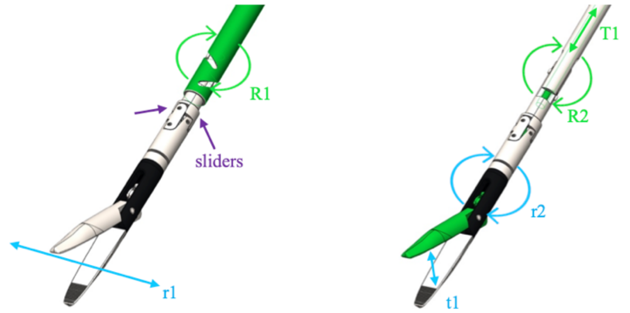

Figure 2, SATA two DOFs BVS instrument and tip, principles of actuation. Left: Sideways articulation (r1) is accomplished by rotation of the outer axis shaft (R1), which drives the sliders. Right: Tip rotation (r2) and opening (t1) are accomplished by rotation (R2) or translation (T3) of the inner axis shaft.

Design goal: Bipolar vessel sealers are generally designed as single use products, while there is a demand for affordable and reusable instruments, both from an economic and sustainable point of view. Although there is a reusable BVS available, the KLS Martin MarSeal, it is not steerable and expensive. In addition, there are no non-robotically controlled BVS instruments with two DOFs available on the market. By being steerable, the user of the instrument is able to deliver a higher quality seal as well as the ability to seal more difficult-to-reach blood vessels and tissue.

In this project, a SATA instrument will be redesigned to sustain bipolar vessel sealing and a new tip will be designed that fits the SATA BVS instrument. To achieve this, options to guide electricity in two directions through the SATA instrument have been explored and drawn into concepts. Separate concepts have been drawn up for the tip. The tip should also facilitate the bi-directional conduction of electricity and serve as a housing for the open- and close mechanism of the jaws. The latter has a strong influence on the design of the tip. The instrument is developed and the most critical parts of the design are identified and evaluated.

The design goal states: ‘’Design a Steerable and Reusable Bipolar Vessel Sealer that is modular, easily disinfected and sterilised and which is reusable for at least thirty surgical procedures whilst maintaining its functionality and assuring patient safety.‘’

Design Method

A number of steps have been taken to work towards the end product. The steps are distributed over three design phases as shown in the flowchart in Figure 3 [12]. In iterative manner, the design steps have been completed repeatedly in order to optimize the product.

Through conducting preliminary research and studying known clinical functioning prerequisites for (bipolar) laparoscopic instruments, the design requirements are specified and design insights are obtained.

In the synthesis phase, ideas are generated and converted into concepts and solutions. In the conceptual developing steps, concepts for the body of the instrument and concepts for the tip are designed independently, as each of these component groups required a different approach.

For the body of the instrument, solutions have been devised as to how electricity can pass through the instrument bi-directionally. For the design of the tip, particular emphasis was placed on the open and close mechanism of the jaws. In the final step of the synthesis phase a detailed CAD model was developed.

As part of the evaluation phase, the design is iteratively optimized during the CAD modelling using FEM simulations. Ultimately, the final design is evaluated on two areas:

1) Lifespan assessment (reusability) by simulating extensive loading on the instrument in FEM (von Mises stress) and combining these results with heavy use (number of cycles) during surgery.
2) The most critical component, the core with its insulating coating, is tested for wear (reusability) in a separate experiment.

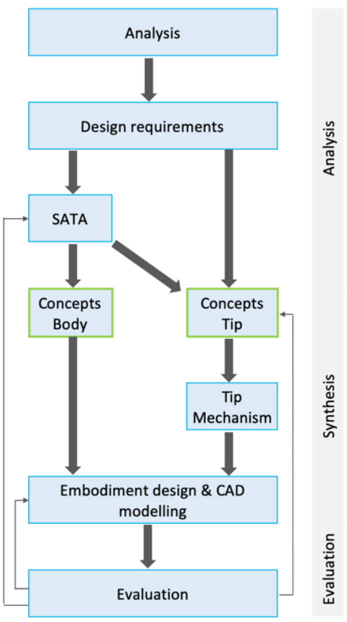

Figure 3, Flow chart design process. The three initial design phases are: analysis, synthesis and evaluation. To go from design goal to end product, a cycle of the three phases is formed as a result of iterative processes. Marked in green are the two sections of the instrument that are separately developed.

Requirements: Developing a Reusable Steerable BVS that fulfils the design goal demands a list of requirements. Medical instruments must be compliant with known clinical functioning prerequisites. The requirements are backed up by literature, manufacturer datasheets, anatomical boundaries and knowledge obtained by consulting engineers and medical staff. Assessment of the concepts and evaluation of the final design is done according to this list. The most crucial design requirements are:

- The instrument must distinguish itself from conventional BVS by being reusable, steerable and modular.
- Seal vessels and tissue in bipolar configuration.
- Apply a uniformly distributed compression of 20N (Fseal) [13].
- Grasp and manipulate tissue [14-16].
- Seal vessels up to 7 mm [15].
- Fit standard trocars for 5 mm instruments [17].
- Be modular and easy to disassemble [18].
- Sterilisable according international standards [14].
- Be reusable for a minimum of 30 surgical procedures [14].
- Limited additional components with respect to current SATA devices [17].
- 2 degrees of freedom in steerability.

Results Design

The final design of the steerable and reusable bipolar vessel sealer is shown in Figure 5. The SATA mechanism has been modified, although both DOFs have been retained as well as the modularity. For the conduction of electricity the existing components have been used and therefore no electrical wires have been added to the instrument. The new tip is bipolar, seals vessels and tissues up to 7 mm and is able to apply a distributed compression force of 20N to the tissue. The seal surface has a length of 20 mm and the distal end of tip allows tissue to be grasped and manipulated. The tip fits seamlessly onto the SATA mechanism. All components and materials used are suitable for steam sterilisation.

Open and close mechanism: The geometry of the open and close mechanism is determined by calculations in Matlab. For this purpose, the dimensioning of a 5 mm instrument was applied and a force Fseal of 20N on a 7 mm blood vessel was chosen as a starting point. Figure 4 shows a sketch of the situation from which the pulling force Ft1 is derived. Pulling force Ft1 is needed to exert a compression force Fseal on the vessel or tissue. Length L1 (see Figure 4) is determined according to a rather extreme situation in which a 7 mm blood vessel is sealed. For optimal force transmission and dimensions of the mechanism it is determined that length L2 = L3 is 4 mm and L4 is 1 mm. The required pulling force Ft1 in this configuration is calculated to be ~50N.

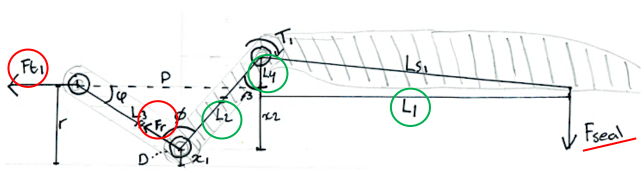

Figure 4, Geometry setup open and close mechanism in Matlab. The Torque T1, resultant force Fr (red), tensile force Ft1 (red), the angles theta and phi and length P are calculated in the fully closed position of the jaws. Variable input for the calculation are lengths L1, L2 and L4 (green).

Figure 5, Renders of CAD model Steerable and Reusable BVS. Top: New tip design without PEEK base. Middle 1st: BVS body plus tip. Middle 2nd: Tip assembly (without coatings) Bottom: Sealing a 7 mm blood vessel. Model documentations are found in Appendix A.

After a series of design iterations the open and close mechanism has been implemented in the design of the BVS as shown in Figure 6. Iterations are mainly based on results obtained through FEM analyses after which the design modifications resulted in a higher safety factor for the included components.

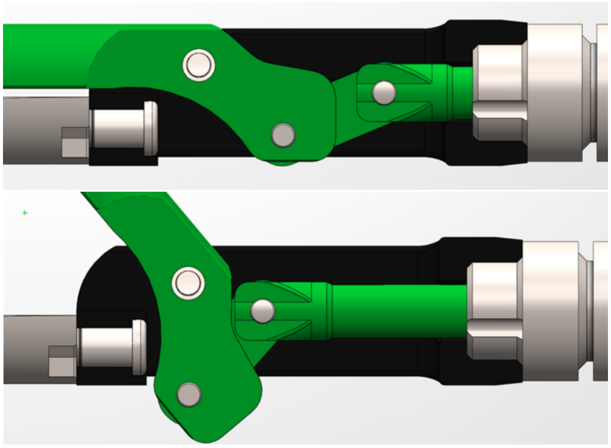

Figure 6, Open and close mechanism 1 in CAD. Top: Fully closed position of the jaws. Bottom: Fully opened position of the jaws.

Active and return electrodes: The composition of the active and return electrodes is shown in Figure 7. The core, open and close mechanism and Upper jaw form the active electrode. The lower jaw and remaining SATA components form the return electrode. Appendix A provides an overview of what components are included in either the active or return electrodes. To achieve distinct electrical paths, electrical insulating (flexible) coatings are applied to the inner axis shaft, nitinol core and NiTiCon component and electrical insulating ceramic coatings are applied to the upper jaw, lower jaw, SS base, tip base, H hinge, sliders high and low and the external axis shaft.

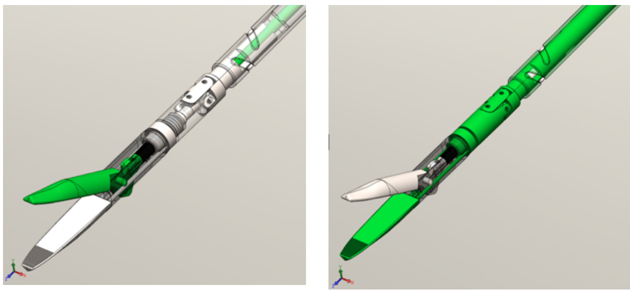

Figure 7, Active and Return electrodes. Left: Active electrode components coloured green. Right: Return electrode components coloured green.

To keep the upper and lower jaws separated, a tip housing made of PEEK designed. PEEK is a polymer and does not conduct electricity. To conduct electricity between the lower jaw and the SATA components (return electrode) there are 2 conductive rods running through the PEEK body, see Figure 5.

Nitinol core for flexibility and steerability: A flexible Nitinol Alloy has been applied for a section of the core. Unlike stainless steel, Nitinol will hardly deform permanently after bending. As shown in Figure 8 below, a piece of Nitinol is attached between two stainless steel components that altogether compose the core.

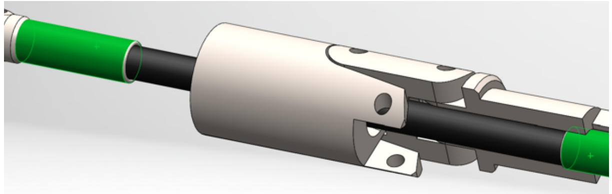

Figure 8, Flexible Nitinol section (black) attached between two stainless steel components (green) composing the core.

Finite Element Method Results

Finite element analysis were performed to assess the design of the BVS. Solidworks simulation (Educational version 2019) software was used for the Finite Element Method (FEM) simulations. Four distinct FEM simulations were performed. Each FEM simulation analysis the individual components within an assembly of components. In this way, the von Mises stress, deformation, displacement and Factor of Safety (FoS) for each individual component is determined. Hinge axis pins are treated as rigid objects. The forces applied in the FEM simulations are derived from the forces obtained from the final geometry section. The simulated components are shown in Table 1 below. A complete report of each FEM simulation is found in Appendix B.

Table 1, Components included in FEM simulations

FEM simulation number	***Component name(s)***
FEM-1	*PEEK base – Lower jaw*
FEM-2	*Upper jaw*
FEM-3	*Connector*
FEM-4	*NiTiCon*

The FoS is calculated using the formula below. The von Mises stress is calculated by FEM, the yield strength (YS) depends on the selected material.

$$FoS = \frac{Yield\ Strength}{max\ von\ Mises\ stress}$$

The selected 316L stainless steel has a YS of 170 MPa and ultimate tensile strength (UTS) of 520 MPa. The selected 30% glass fiber reinforced PEEK has a YS = UTS of 158 MPa.

FEM walkthrough and results: A similar protocol has been applied to every FEM simulation. First of all, the simulation was set up by defining materials, connections and constraints. Subsequently, simulations were run with two different magnitudes of forces:

1) The applied forces Fr and Ft1 are derived from the earlier Matlab calculations to seal a blood vessel of 7 mm with a compression force Fseal of 20N.
2) Where the forces Fr and Ft1 are increased with respect to option 1), in order to obtain a certain design Safety Factor >1.5 [19].

Figure 9 shows the setup of FEM-1 as an example. The green icons are constraints, in this case the PEEK component fixed to the environment in the most proximal surfaces. The purple arrows indicate the applied force, in this case a uniformly distributed compression force of 20N. Furthermore, the bolt has been simulated and evaluated by the simulation software to determine its safety factor and axial pre-load.

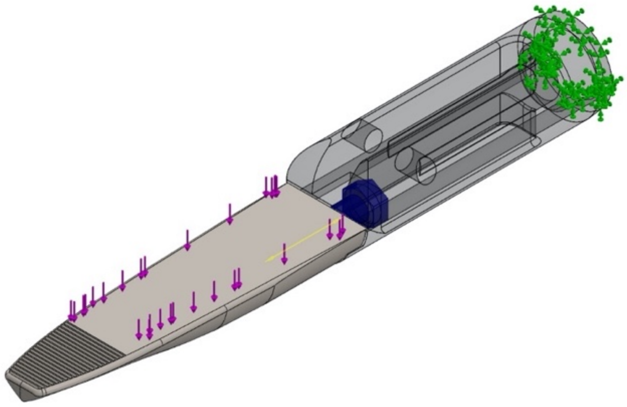

Figure 9, Setup FEM-1. Distributed force Fseal is applied to the first 15 mm of the lower jaw's surface. Blue coloured is the simulated bolt connector. The PEEK base is fixed at the most proximal surfaces

The most valuable outcomes in these simulations are the von Mises stress. Based on these stresses, the design is evaluated on component level and an estimation of the lifespan is ultimately determined. The FEM process and a component evaluation has been exemplified through FEM-2.

FEM-2: Two similar simulations were run in which the applied force (Fr) was either 55N or 69N, see Figure 10 and Figure 11 respectively. In both cases, the maximum stress is higher than the allowable stress for a safety factor of >1.5 and in the case of Fr = 69N, the maximum stress is higher than yield strength (170 MPa) of 316L stainless steel. Zooming in on the stress concentrations, it is shown that these stresses will most likely not cause component failure.

Figure 12 shows the first couple of element rows around the holes where the upper jaw and connector component are connected via a hinge pin. The stress progression from high (purple) to low (green) is visible whereby the stress in the 2nd row of elements (below holes surface) is low enough for a safety factor of >1.5. The graph in Figure 13 shows more clearly that when the stress falls below 113.3 MPa, a safety factor of >1.5 applies. This shows that the high stress does not penetrate deeper into the material.

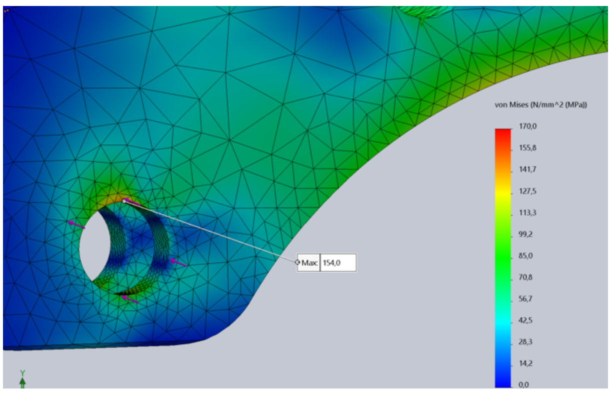

Figure 10, Stress concentration surrounding the holes. The applied force Fr was 55N and maximum stress 154 MPa.

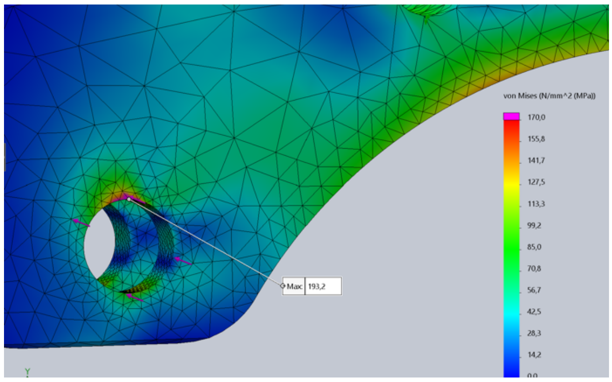

Figure 11, Stress concentration surrounding the holes (coloured purple). The applied force Fr was 69N and maximum stress 193.2.

In the case of stresses higher than yield strength, further material fatigue analysis was carried out to determine how many repeated cycles the component can be subjected to the equally high stress before damage occurs. In similar way, the other components are approached and evaluated, see Appendix B.

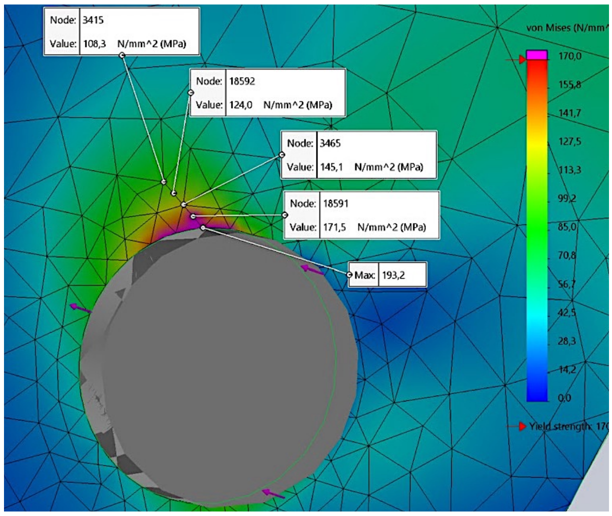

Figure 12, Four nodes and the maximum that show stress degradation. The probe function in Solidworks is used to obtain this figure. The probed notes correspond to the notes in Figure 13 below

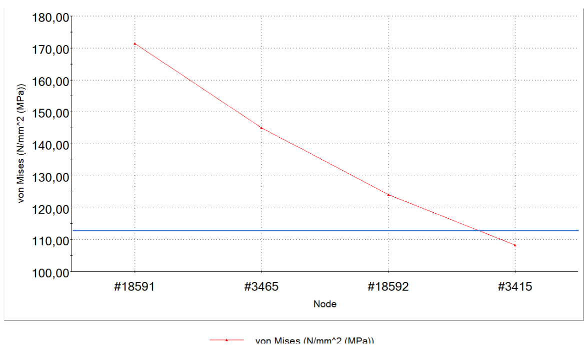

Figure 13, Graph of the stress development through the first two rows of elements. Starting point on the left is the node in the middle of the first element. End point to the right is a first node of the third row of elements. The blue line at ~113.3 MPa is the boundary for which holds that below the line FoS > 1.5.

PEEK component: If the PEEK component is isolated from FEM-1, a maximum stress of 114.2 MPa is obtained, see Figure 14. The maximum allowable stress for an unreinforced PEEK is around 100 MPa, however for a specific 30% glass fiber reinforced PEEK this is around 158 MPa. If a glass fiber reinforced PEEK is selected, the stress must be below 105 MPa to obtain a safety factor of >1.5. Higher stress occurs near the corners around the central cut out, i.e. where the open- and close mechanism fits in between. Therefore a fatigue test should determine if the component will fail due to fatigue. It must be noted that in reality the rigidity of the PEEK component is slightly increased by adding the metal conductive rods. In any case, a reinforced PEEK is required.

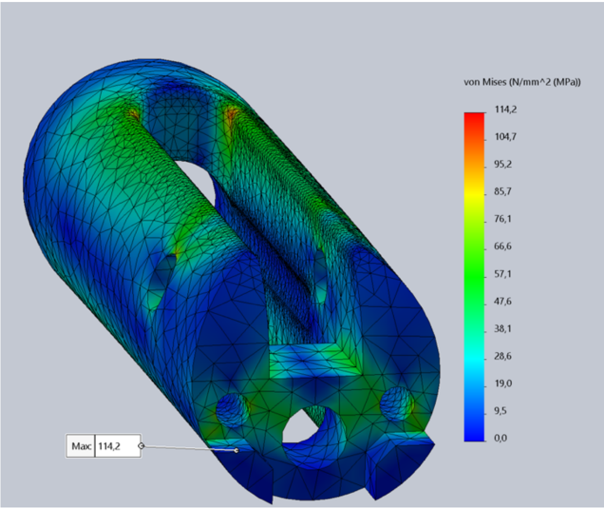

Figure 14, FEM-1 von Mises stress PEEK base. Maximum stress is 114.2 MPa.

Estimated lifespan: *One of the* design requirements states that an instrument must be reused for at least thirty surgical procedures. The number of cycles in each of these surgical procedures is likely to vary widely because it is dependent on influencing factors such as, type of procedure and experience level of the surgeon. Meeuwsen et al. (2017) investigated the variety of differences in usage of electrosurgical devices. Part of their study focused on the number of activations of an electrosurgical device during cholecystectomies (these procedures have a relatively standard execution [20]). According their data [20], the mean number of activations is 102.

Multiplying the mean number of activations/cycles (102) with the minimum amount of surgical procedures (30), results in a total cycle number of 3060. In other words, each BVS must withstand a minimum of 3060 cycles without any fatigue failure occurring. In the worst-case scenario, the instrument is activated >200 times during thirty procedures, resulting in a total of 6000 cycles. The possible occurrence of fatigue failure can be derived from fatigue diagrams, also known as S-N curves see Figure 15.

The maximum stress (peak stress) of each of the components obtained from the FEM analysis can be added to the S-N curve to determine if fatigue failure occurs and, if so, after how many cycles. If the peak stresses are too low, no fatigue failure will occur. This holds for components 5 (Connector) and 6 (NiTiCon).

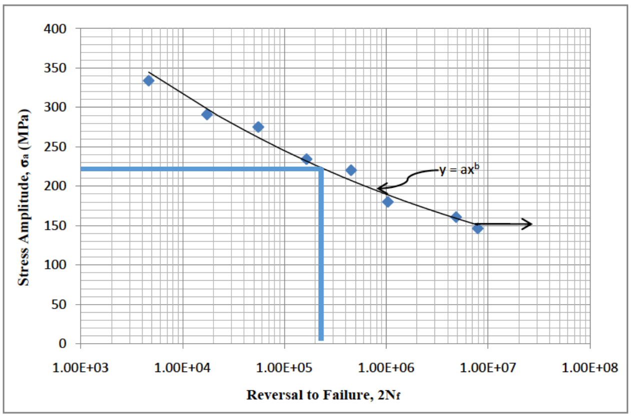

Figure 15, S-N curve 316L stainless steel316L [21]. Peak stress obtained from FEM-1 are inserted

The highest peak stresses were obtained in FEM-1, where the lower jaw shows stress concentrations of ~214 MPa. The lower jaw's fatigue life is estimated at 350 000 cycles according Figure 15. Second highest stresses were obtained in FEM-2, the upper jaw. Peak stresses of ~193 MPa occurred. Both well exceed the required lifespan (cycles), thus is it concluded that the components will not fail due to fatigue. Eventually it must be taken into consideration that there are other factors that can affect the fatigue life, such as corrosion and temperature.

Core Coating Validation

An experiment was conducted to measure the durability of a Nitinol Alloy guidewire with PTFE coating pulled through various SATA hinges. The experiment was conducted in the form of several pilots, in this way it was quickly determined whether the design solution is feasible and what should be considered in future research and future designs.

Materials: A complete initial test setup is provided in Figure 16, using this set up pilot 1 has been performed. An adjustment to this set up has been made for pilot 2 and 3, Figure 17.

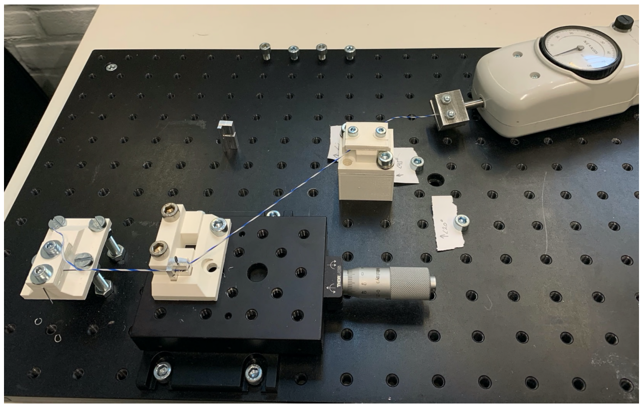

Figure 16, Test setup. The guidewire (core) is currently clamped, under preload, on both ends. The core is always clamped on the left (distal / tip) end. Then the guidewire runs through the mimicked SATA hinge, with either 45 or 70 degrees as a fixed angle. The linear stage is moved 4 mm to the left, simulating a full jaw closure movement. On the right side (proximal / handle), the guidewire is attached to the force gauge.

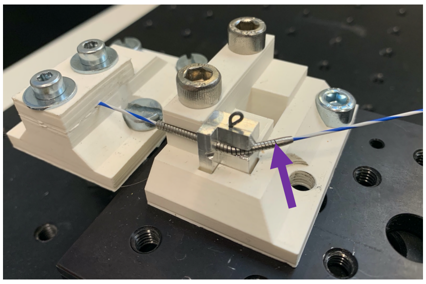

Figure 17, Additional stainless steel flexible overtube.

Instruments & equipment:

- A 5 mm laparoscopic SATA instrument by Surge-On Medical, Delft, Holland was used to obtain CAD models.
- A Bavarian Wire guidewire manufactured by Medi-Globe GmbH, Achenmühle, Germany consist of Nitinol Alloy cores with PTFE coating. For this experiment a core diameter of 0.889 mm (including the coating) was used.
- A handheld mechanical force gauge by Chatillon, was used to establish and maintain the preload/ applied load.
- A digital multimeter by STREX was used to measure possible current between the guidewire and aluminium angle block.
- A linear translation stage by Thorlabs, Newton, US, was used to precisely mimic the linear travel distance the core makes during a full open-to-close movement of the jaws.
- From a SATA instrument 3D CAD file, two steering angles were defined and corresponding surfaces were extracted. Based on these surfaces, 2 aluminium blocks have been milled that mimic the SATA instrument under angle during the experiment, Figure 18.
- The 'angle block' housing and core clamps are 3D printed out of PLA.

Figure 18, Aluminium 'angle blocks'. Left: 45 degrees angle at slider High side with hinge axis pin. Right: 70 degrees angle at slider low and H hinge side. There is no interference of the hinge pin while steering in this direction.

Experimental design: Two types of variables are distinguished, namely dependent and independent variables. The *electrical resistance* is the dependent variable. The resistance is measured between the Nitinol core and the aluminium angle block. When a resistance is registered by the multimeter, it means that the insulating PTFE coating has failed. I.e. current is leaking between the nitinol core and the aluminium angle block. The independent variables are: the *angles* of the SATA mechanism (45º and 70º), *preload* of the core (15N – 60N) and *linear translation* of the core (4 mm). Three distinctive pilots were conducted:

Pilot 1) In this setup, the guidewire is pulled directly through the aluminium 'angle blocks', which means that the guidewire is in contact with the aluminium at one or two points. These contact points are considered critical points, around which the PTFE coated Nitinol guidewire bends and where most of the coating's wear occurs.

Pilot 2)
The wear on the coating is reduced by adding a flexible torque coil to the hinge, i.e. overtube. The overtube, through which the guidewire is pulled, ensures that the forces acting on the guidewire are evenly distributed by replacing the critical contact points with a larger contact surface. Furthermore, using an overtube increases the bending radius and eliminates sharp edges. For this pilot, a stainless-steel flat torque coil was used.

Pilot 3) Building on pilot 2, pilot 3 was used to investigate after how many repeated cycles damage occurs to the PTFE coating under certain conditions.

Protocol: Sealing a blood vessel is considered as one cycle. A cycle is defined as: the complete closing of the jaws, which requires a core translation of 4.0 mm and a constant load during the cycle. Irrespective of the pilots and specimen, experimental cycles were done according the protocol outlined in Table 2. A variety of pulling forces is applied. Approximately 50N corresponds to the force required to apply compression of 20N with the jaws, however, the effect of lower and higher forces has also been studied.

Table 2, Protocol for one experimental cycle to evaluate the Nitinol PTFE coated guidewire.

1	*Select the desired 'angle block' and slide it into its fixed position*
2	*Set the linear stage to 0 mm*
3	*Stick the specimen though both the 'angle block' and clamp and screw tight the clamp.*
4	*Set the multimeter to continuity test mode (audio que) or resistance mode and connect the red and black electrodes to the nitinol and aluminium 'angle block'*
5	*Check if the force gauge is calibrated at zero, pull in the corresponding angle direction and manually apply a force of ~50N.*
6	*Maintain the tensile force whilst moving the linear stage 4 mm.*
7	*Release applied force and return the linear stage to its starting position.*
8	*Repeat the cycle until the multimeter registrates a resistance or continuity.*

Results core coating test

Three pilots have been conducted:
Pilot 1): In the first pilot a total of six cycles have been conducted. After step 6 (see protocol), the guidewire was clamped on both ends, thus maintaining the applied load, before measuring the resistance. Insulation failure was measured after each cycle in pilot. The damage was also observed visually after each cycle. Figure 19, shows the visual damage after the first cycle. After applying the preload of 60N at the start of cycle 5 insulation failure occurred immediately, see Figure 20.

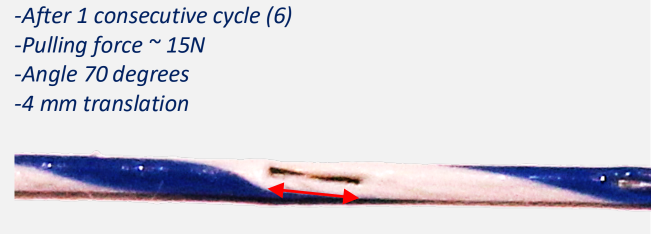

Figure 19, Coating damage pilot 1, cycle 6.

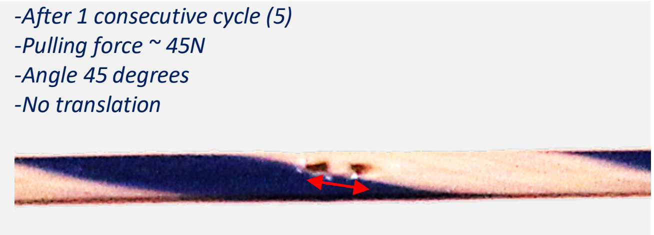

Figure 20, Coating damage pilot 1, cycle 5.

Pilot 2): After adding an overtube to the test setup, a second pilot containing eight cycles was conducted. Cycle 2 and 8 caused insulation failure and showed visual damage, see Figure 21 below. With the angle <= 45° there was no measurable or visual damage after 1 cycle.

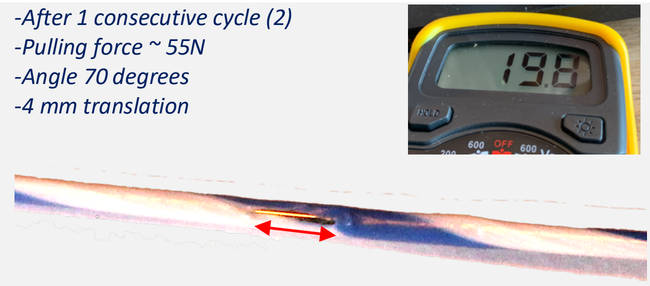

Figure 21, Coating damage pilot 2, cycle 2. Multimeter detects current and measures a resistance.

Pilot 3): The last pilot consisted of five runs of cycles. A total of fifty-four cycles were performed. The multimeter was connected continuously and set to continuity. Figure 22 and Figure 23, show the most promising results obtained from the third run.

At an angle of 70°, measurable and visible damage occurred after minimum 4 to maximum 11 cycles. 45° with axis pin showed measurable and visible damage after a minimum of 4 and maximum of 5 cycles.

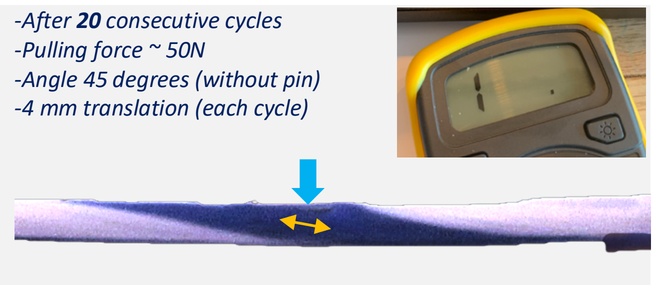

Figure 22, Coating wear near rupture during run 3.2. Yellow arrow indicates area where coating has suffered severe wear. Insulation was sufficient not to measure a closed circuit with the multimeter. (The multimeter displays 1 ., when there is no current flowing).

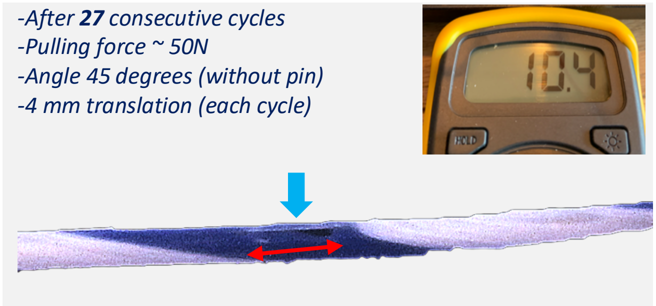

Figure 23, Insulation failure during run 3.3. Multimeter detected insulation failure during the 7th cycle in run 3.3. This was after 27 consecutive cycles

Discussion

An essential instrument used during MIS is a BVS. Most BVS instruments currently on the market are single-use products. Particularly in LMICs, the use of single-use instruments is often not financially feasible, and the cleaning and sterilization possibilities of complex reusable instruments are limited. The first part of the design goal was to develop a BVS that is modular, easy to clean and sterilised and therefore reusable. SATA provides the basis for the instrument that is steerable and optimized for reusability. Therefore, the second part of the design goal was to implement the functionalities of a BVS into a SATA instrument to obtain a BVS that is steerable and reusable. To achieve the design goal, modifications to the SATA instrument have been made in order to safely conduct electricity from and to the tip. In addition, a new tip has been designed that is inspired by existing BVS on the market. The tip fits seamlessly onto a SATA instrument whilst maintain its steerable functionalities and reusability.

The choice of the 'core model' concept for the instrument body results from the evaluation of the concepts through Harris profiles which is based on the design requirements. Particular attention has been paid to the conduction of electricity through the shafts of the instrument. In the case of the 'Core model', minimal modifications to the current SATA components is required, few additional components have been added to the design and the concept is partly derived from existing design solutions.

A number of aspects needed to be investigated further to obtain a decisive tip design, such as the insulating layers and the open and closing mechanism of the jaws. A proven principle has been chosen for the tip insulation, i.e. making the complete tip housing from PEEK. On grounds of current research into ceramic coatings [11], it cannot be substantiated whether their use as an insulating layer or insert between the upper and lower jaws is suitable. Decisive for the tip design was the choice for the particular open and close mechanism. It must be noted that during calculations of the mechanism not all forces were taken into account, such as frictional forces in the hinges or forces in y-direction. How much effect these forces have on the required tensile forces can be investigated further. In addition to satisfactory results obtained through calculations, it was found during early design iterations that the open and close mechanism was readily implementable in the design of the tip. On the contrary, problems arose with the implementation of two other mechanisms due to construction interferences.

For calculating the required tensile force Ft in the core, the distance (L1) between the rotation point of the upper jaw and the point of application of the sealing force Fseal has the biggest influence. First, the method used to determine L1 and Ft1 is based on a rather extreme schematic configuration. Although sealing blood vessels up to 7 mm is seen as a benchmark for BVS instruments by manufacturers [22], a blood vessel with a diameter of 7 mm is in most cases larger than the vessels and tissues that are sealed in practice. The compression force Fseal of 20N is a maximum required to seal a blood vessel of 7 mm in diameter. For smaller tissues a Fseal < 20N may be sufficient to obtain a high quality seal [13]. Furthermore, a blood vessel is never perfectly round and often branches of vessels are sealed as well. Nevertheless, using this extreme configuration as a reference will contribute to strengthening the components more than would be required in practice. Second, an additional safety factor was obtained by introducing forces based on length L1 = 12.5 mm. Although in reality it is assumed that the user of the instrument will most likely clamp the blood vessels as proximally as possible between the jaws, for which L1 corresponds to a length of 9.95 mm for a 7 mm vessel. However, higher forces obtained with L1 = 12.5 were applied during FEM simulations to optimise the design. In short, both the extreme configuration and the extended L1 lead to a higher safety factor. And thus a stronger design in which misuse will less likely to lead to instrument failure.

Grasping and manipulation of tissues, where a force Fseal of 7N must be applied at the most distal point of the tip (L1 = 25 mm) using mechanism 1, will in no case result in a higher required tensile force Ft than for sealing with 20N and an L1 of 9.95 mm or 12.5 mm. However, the grasping and manipulation of tissues must be counted as one cycle for determining the lifespan of the components in question, because the forces Fr and Ft are similar in the case of sealing and grasping or manipulation.

The validation of the design was done in two ways: 1) By performing stress calculations and simulations of some tip components using FEM in SolidWorks and by approximating the expected lifespan of these tip components. 2) By studying the wear of a PTFE coating on a Nitinol wire, which is seen as the most critical component in the new BVS.

FEM design evaluation: FEM simulations have been performed continuously during the design iterations of the tip. In these simulations, the components of the tip and in particular the open and close mechanism are engineered such that they obtained a safety factor of > 1.5. If a safety factor > 1.0 is present, the maximum stresses are always lower than the permissible yield stresses of the material. In this case it is very unlikely that fatigue will occur and the life span is > 1.0 * 10^ 6 cycles. Concerning the stainless-steel components in the tip, the expected lifespan is much longer than the required lifespan of the components. Therefore, it is assumed that the design is strong enough.

For the PEEK component the highest stresses are 114 MPa with a Fseal of 20N on a blood vessel of 7 mm. The tensile strength of unreinforced PEEK is known to be close to 100 MPa. The use of unreinforced PEEK will consequently have a safety factor of < 1.0 and is therefore not recommended. The solution is a 30% glass-fibre reinforced PEEK. This material offers a higher tensile strength of up to 160 MPa, a higher stiffness and is therefore more suitable for structural purposes. Just like normal PEEK, glass-fibre reinforced PEEK is also suitable for injection moulding, extrusion and machining and its properties such as wear resistance, chemical resistance and sterilisation-ability make this material suitable for healthcare applications, such as a BVS.

Core coating evaluation: The feasibility of the concept in which the core is part of the active electrode falls or stands on the insulating coating around the core. Nitinol has already proven itself to be a suitable material for components requiring torsional stiffness and flexibility.

The setup for Pilot 1 was initially designed for a larger experiment in which the coating was extensively tested under different conditions, such as different angular positions of the SATA hinge and variable tensile forces and rotations of the core. However, the PTFE coating on the guidewire is engineered for a different application. In fact, it is a hydrophilic coating designed to have a very low coefficient of friction, but this makes it very soft and hardly wear resistant. The two contact points over which the coating scrapes and the angle that the hinge makes are sharp enough to have the PTFE coating immediately damaged upon translation. Even without translation, as in Figure 20, the coating already ruptures under due to applied force. In this case, the coating cracked at the point where it contacts the axis shaft. Also applied forces (15N), much lower than the required tensile forces (50N), caused damage to the coating. A solution for this problem was sought by adding an overtube. The results of this were obtained from pilot 2 and 3. By using an overtube, the core will be pulled over a contact area instead of contact points as mentioned before. The contact surface provides a more uniformly distributed load on the core and the bending radius that the core has to make through the SATA hinge is larger and more constant, which decreases the wear of the coating.

Run three (pilot 3) showed the most promising results. An angle of 45 degrees was selected, but without inserting the hinge pin. The force applied was ~50N. No visible damage was seen after the first set of ten cycles. At the end of the second run, the coating was noticeably deformed, but there was no insulation failure as can be observed in Figure 22. During the third set, the coating eventually ruptured in cycle 7, see Figure 23.

Damage to the insulating coating occurs relatively fast at an angle of 45 degrees with hinge axis pin compared to cycles where the hinge axis pin is removed. Because the pin lies partly in the path of the core, this inevitably forms a critical point were the guidewire will bend and kink. Even after adding an overtube, damage to the PTFE coating occurs much quicker at this specific point. As expected, damage occurs comparatively faster when the angle is 70 degrees than with an angle of 45 degrees without a hinge axis pin.

It should be emphasized that, despite the promising (improved) results of using an overtube, insulation failure of the coating after 27 cycles is far from satisfactory for a reusable instrument. In fact, 27 cycles are not even sufficient for the duration of a single surgical procedure, i.e. >100 cycles.

Recommendations: Research into a more wear-resistant PTFE coating or a replacement material is strictly necessary. The main purpose of the currently tested PTFE coating on the guidewire is to achieve the lowest possible friction, but the guidewire has a completely different application than the core with a PTFE coating in the design of a BVS. Although low friction of the insulation layer around the core in the BVS is also desirable, this is not the most important function. Low friction between the core and other components can also be achieved by coating the other components with, for example, a ceramic coating that also has a low coefficient of friction. It is also possible to choose a replacement material for PTFE, whereby these materials are in any case wear-resistant, highly flexible, electrically insulating and sterilisable.

There are various options for the overtube in terms of shape and material. Initially, a suitable overtube must be sought and tested which is compatible with the current SATA mechanism design. Figure 24 shows an example of an overtube incorporated in the BVS CAD design. It is essential to test the overtube in combination with a more wear-resistant insulating coating. Furthermore, it is possible to make the overtube part of the steering mechanism. For example, the overtube can be attached to the stainless-steel part of the core (inner shaft axis) and the stainless-steel part of the tip (SS base) to provide more torsional stiffness required to rotate the tip around its longitudinal axis.

Figure 24, Stainless steel overtube. A cross section of the SATA tip base component containing an overtube of 2 mm in diameter and a length of ~10 mm. The component is not fixed but held in place by the screw component of the tip (SS base), the SATA tip base and both sliders. This ensures that the modularity is retained and cleaning is accessible. Furthermore, the component can easily be replaced when necessary.

The pilot experiments showed that at one side of the instrument the axis pin of the SATA hinge crosses the path of the core when the SATA hinge is articulated. In effect, the pin presses against the overtube and creates a point load instead of an evenly distributed load. Simultaneously, the bending radius of the overtube and thus the core is very small when the SATA hinge is articulated to this side of the device. It is recommended to re-design the SATA mechanism in such a way that the bending radius is increased and the pin is no longer crossing the path of the core when the SATA hinge is articulated.

As indicated earlier, more research is needed into the exact composition and deposition methods of the ceramic electrically insulating coatings and their properties in practice. A possible area of this research could be aimed at searching for coatings that both insulate and provide an anti-stick layer. An anti-stick layer ensures that coagulated tissue does not stick to the jaws very easily and reduces the chance of tissue clogging. As a results, the seal quality remains higher during the surgical procedure and it furthermore it provides extra ease of use.

This thesis focuses on the shafts of a SATA instrument and the tip. In the future, modifications to the current design of the SATA handle will be necessary to enable the electricity to pass through the handle and for connecting the instrument to a bipolar electrosurgical generator. In Furthermore, the mechanical design of the handle is key to ensure that the pulling force on the core is limited and not much higher than the calculated pulling force Ft, thus preventing any damage.

Conclusion

The design goal for this thesis project was to develop and evaluate a novel Steerable and Reusable Bipolar Vessel Sealer incorporated into an instrument with Shaft Actuated Tip Articulation technology. With the introduction of a reusable instrument, costs in particular must be reduced to ensure that this type of laparoscopic instrument becomes more accessible for use in low- and middle-income settings. In addition, reusable instruments contribute to sustainable surgery and thus a sustainable healthcare.

The results were achieved by redesigning a SATA instrument and making it suitable for Bipolar energy transmission. Where possible, existing components of the SATA instrument are part of the active and return electrodes and together with a new tip design, this ensures a closed circuit when tissues and blood vessels are clamped by the jaws. Strategically applied insulating coatings prevent short circuiting and collateral tissue damage. Simultaneously, an ideal uniformly distributed pressure of 20N can be applied on the tissue. All together, these properties ensure that the final model meets the requirements of functioning as a BVS.

The new design of the tip is as simple and robust as possible and fits seamlessly into the existing SATA instruments. Limited additional components are introduced by the new design and the modularity is retained. Used materials are suitable for repeated cleaning, disinfection and sterilization cycles. Therefore, the current design has the potential to be reused for many surgical procedures and thus, after further development, an instrument will be delivered that indirectly contributes to reducing costs and making healthcare more sustainable.

References

[1] T. Horeman, M. Aguirre, Jr., G. M. M. J. Kerkhoffs, J. Dankelman, and G. M. J. Tuijthof, "The SATA, A Simple, Stiff, and Rigid Steering Mechanism1," *Journal of Medical Devices,* vol. 9, no. 3, 2015, doi: 10.1115/1.4030564.

[2] J. C. Hu *et al.*, "Comparative effectiveness of minimally invasive vs open radical prostatectomy," *Jama,* vol. 302, no. 14, pp. 1557-1564, 2009.

[3] R. J. Verhage, E. Hazebroek, J. Boone, and R. Van Hillegersberg, "Minimally invasive surgery compared to open procedures in esophagectomy for cancer: a systematic review of the literature," *Minerva chirurgica,* vol. 64, no. 2, p. 135, 2009.

[4] V. Mouraviev *et al.*, "Financial comparative analysis of minimally invasive surgery to open surgery for localized prostate cancer: a single-institution experience," *Urology,* vol. 69, no. 2, pp. 311-314, 2007.

[5] M. Wani, M. Shahdhar, and U. Sheikh, "Transumbilical SILC Using Conventional Laparoscopic Instruments—Initial Experience in a Resource-Limited Setting," *Indian Journal of Surgery,* vol. 77, no. 2, pp. 624-627, 2015.

[6] T. E. Chao, M. Mandigo, J. Opoku-Anane, and R. Maine, "Systematic review of laparoscopic surgery in low-and middle-income countries: benefits, challenges, and strategies," *Surgical endoscopy,* vol. 30, no. 1, pp. 1-10, 2016.

[7] J. Siu, A. G. Hill, and A. D. MacCormick, "Systematic review of reusable versus disposable laparoscopic instruments: costs and safety," *ANZ journal of surgery,* vol. 87, no. 1-2, pp. 28-33, 2017.

[8] Medtronic, October 26, 2020. [Online]. Available: https://www.medtronic.com/covidien/nl-nl/products/vessel-sealing/ligasure-blunt-tip-sealer-divider.html#.

[9] G. Kane, C. Bakker, and A. Balkenende, "Towards design strategies for circular medical products," *Resources, Conservation and Recycling,* vol. 135, pp. 38-47, 2018.

[10] M. Minoglou, S. Gerassimidou, and D. Komilis, "Healthcare waste generation worldwide and its dependence on socio-economic and environmental factors," *Sustainability,* vol. 9, no. 2, p. 220, 2017.

[11] P. d. Haes, "Electrical conductive and insulating coatings as a replacement for conventional wires in bipolar electrosurgical instruments, a systematic review on coatings and their properties.," 2020.

[12] N. F. Roozenburg and J. Eekels, "Product design: fundamentals and methods," 1995.

[13] R. Lether, "Bipolar Electrosurgical Graspers, A Literature Study," 2020. Faculty of Mechanical, Maritime and Materials Engineering (3mE) · Delft University of Technology.

[14] S. Manasnayakorn, A. Cuschieri, and G. Hanna, "Ideal manipulation angle and instrument length in hand-assisted laparoscopic surgery," *Surgical endoscopy,* vol. 22, no. 4, pp. 924-929, 2008.

[15] E. Heijnsdijk, H. De Visser, J. Dankelman, and D. Gouma, "Slip and damage properties of jaws of laparoscopic graspers," *Surgical Endoscopy and Other Interventional Techniques,* vol. 18, no. 6, pp. 974-979, 2004.

[16] E. Heijnsdijk, A. Pasdeloup, A. Van der Pijl, J. Dankelman, and D. Gouma, "The influence of force feedback and visual feedback in grasping tissue laparoscopicaUy," *Surgical endoscopy,* vol. 50, no. 1, pp. 980-985, 2004.

[17] S. F. Hardon, F. Schilder, J. Bonjer, J. Dankelman, and T. Horeman, "A new modular mechanism that allows full detachability and cleaning of steerable laparoscopic instruments," *Surgical endoscopy,* vol. 33, no. 10, pp. 3484-3493, 2019.

[18] T. Horeman, F. Schilder, M. Aguirre, G. Kerkhoffs, and G. Tuijthof, "Design and preliminary evaluation of a stiff steerable cutter for arthroscopic procedures," *Journal of Medical Devices,* vol. 9, no. 4, 2015.

[19] M. Brousseau and O. Manager, "IEC 60601-1 3rd Edition Risk Management Requirements and Product Design," *Medical Design Technology,* p. n/a, 2015.

[20] F. C. Meeuwsen, A. C. Guédon, E. A. Arkenbout, M. van der Elst, J. Dankelman, and J. J. van den Dobbelsteen, "The art of electrosurgery: trainees and experts," *Surgical innovation,* vol. 24, no. 4, pp. 373-378, 2017.

[21] K. Mohammad, A. Ali, B. Sahari, and S. Abdullah, "Fatigue behavior of austenitic type 316L stainless steel," in *IOP conference series: materials science and engineering*, 2012, vol. 36, no. 1: IOP Publishing, p. 012012.

[22] R. W. Timm, R. M. Asher, K. R. Tellio, A. L. Welling, J. W. Clymer, and J. F. Amaral, "Sealing vessels up to 7 mm in diameter solely with ultrasonic technology," *Medical Devices (Auckland, NZ),* vol. 7, p. 263, 2014.

Appendixes

A) **Model Documentation**
B) **FEM reports**

A) CAD model documentation

All component names, numbers and description are included in Table A-1. A distinction is made between the components in the tip and components for the SATA mechanism. Table A-2 includes the components that are part of either the active electrode or return electrode. For all the components suggested materials have been added in Table A-3, as well as possible manufacturing methods and whether the components are coated.

Table A-1, Components list final model reusable and steerable bipolar vessel sealer.

Component number	**Name component**	**Component description**	**Quantity**
TIP			
1	PH_4000_v8 – SS base	Threaded tip base bonded with PEEK base	
2	PH_4001_v8 – PEEK base	Polymer tip housing	
3	PH_4002_v8 – Lower jaw	Lower jaw	
4	PH_4003_v8 – Upper jaw	Upper jaw	
5	PH_4004_v8 – Connector	Link between Upper jaw and Core	
6	PH_4005_v8 – NiTiCon	Distal end of the core, to connect Nitinol rod with connector	
7	PH_4006_v8 – Conductor rod	Electrically conductive rods, connecting the Lower jaw with the SS base	II
8	PH_4007_v8 – PIN	Bolt that connects the PEEK base with the Lower jaw	
9	PH_4008_v8 – Axis UJ	The Upper jaw axis	
10	PH_4009_v8 – Axis UJ insert	To hold in place the UJ axis.	
11	PH_4010_v8 – axis pin (2mm)	Axis between Upper jaw and Connector	
12	PH_4011_v8 – axis pin (2mm) round	Axis between Connector and NiTiCon	
13	PH_4012_v8 – Nitinol rod	Flexible part of the core	
14	PH_4013_v8 – Nitinol rod insulation	Flexible insulation for the core	
15	PH_4014_v8 – Overtube	Flexible core protection rod	
16	PH_4015_v8 – PEEK overtube	Additional insulation to prevent short circuiting	
SATA			
17	PH_011 – External axis shaft	Outer shaft with ceramic insulation coating	
18	PH_012 – Mid axis shaft	Middle shaft, housing the core	
19	PH_013 – Inner axis shaft	Core	
20	PH_031 – Tip base_revised_smooth	Threaded base (nut)	
21	PH_032 – H hinge - revised	Connecting the Slider low with tip base	
22	PH_033 – Slider high - revised	Directly connected to the tip base	
23	PH_034 – Slider low - revised	Connected to the H hinge	
24	PH_041 – Slider pin	Slider pin's run through a guided path in the External axis shaft.	II

Table A-2, Components that are part of the active and return electrodes.

(Name and component number)	
Active electrode:	**Return electrode:**

Inner axis shaft	*19*	*Lower jaw*	*3*
Nitinol core	*13*	*Conductor rods*	*7*
NiTiCon component	*6*	*SS base*	*1*
Connector	*5*	*Tip base*	*20*
Upper jaw.	*4*	*(Overtube)*	*15*
		H hinge	*21*
		Slider high	*22*
		Slider low	*23*
		Mid axis shaft	*18*

Table A-2, Materials, coating and manufacturing methods.

Component number	***Material description***	***Manufacturing method***	***Coating applied***	***Coating type***
1	*Stainless Steel 316L*	*Extrusion + conventional*	*Yes*	*Ceramic insulation*
2	*30% Glass Fibre reinforced PEEK*	*Injection moulding, Extrusion*		
3	*Stainless Steel 316L*	*Moulding + conventional*	*Yes*	*Ceramic insulation + Anti stick*
4	*Stainless Steel 316L*	*Moulding + conventional*	*Yes*	*Ceramic insulation + Anti stick*
5	*Hardened Stainless Steel 316L*	*Extrusion + conventional*		
6	*Stainless Steel 316L*	*Extrusion + conventional*	*Yes*	*PTFE insulation*
7	*Hardened Stainless Steel 316L*	*Extrusion + conventional*		
8	*Hardened Stainless Steel 316L*	*Extrusion + conventional*		
9	*Hardened Stainless Steel 316L*	*Extrusion + conventional*		
10	*Hardened Stainless Steel 316L*	*Extrusion + conventional*		
11	*Hardened Stainless Steel 316L*	*Extrusion + conventional*		
12	*Hardened Stainless Steel 316L*	*Extrusion + conventional*		
13	*Nitinol Alloy*	*Extrusion + conventional*	*Yes*	*See component 14*
14	*PTFE or PVDF*			
15	*Stainless Steel 316L*	*Extrusion, laser cut*		
16	*PEEK*	*Extrusion + conventional*		
17	*Stainless Steel 316L*	*Extrusion + conventional*	*Yes*	*Ceramic insulation*
18	*Stainless Steel 316L*	*Extrusion + conventional*		
19	*Stainless Steel 316L*	*Extrusion + conventional*	*Yes*	*Ceramic or polymer*
20	*Stainless Steel 316L*	*Extrusion + conventional*	*Yes*	*Ceramic insulation*
21	*Stainless Steel 316L*	*Extrusion + conventional*	*Yes*	*Ceramic insulation*
22	*Stainless Steel 316L*	*Extrusion + conventional*	*Yes*	*Ceramic insulation*
23	*Stainless Steel 316L*	*Extrusion + conventional*	*Yes*	*Ceramic insulation*
24	*Hardened Stainless Steel 316L*	*Extrusion + conventional*	*Yes*	*Ceramic insulation*

An overview of all connections are shown in Table A-4 below. If necessary, the same connections were included in the setup of the respective FEM simulations in the next section. Connection types are recommended but not definitive. The hinge connections for the open- and close mechanism and SATA mechanism are excluded.

Table A-4, Connections between components.

Connection number	***Component A***	***Component B***	***Connection type***
C1	*SS base*	*PEEK base*	*Adhesive*
C2	*PEEK base*	*Lower jaw*	*Threaded bolt*
C3	*PEEK base*	*Lower jaw*	*Adhesive*
C4 – C5	*SS base*	*Conductor rod*	*Welding + adhesive*
C6 – C7	*Lower jaw*	*Conductor rod*	*Welding + adhesive*
C8 – C9	*PEEK base*	*Axis UJ*	*Adhesive*
C10 – C11	*PEEK base*	*Axis UJ insert*	*Adhesive*
C12	*Axis UJ insert*	*UJ axis*	*Spot welding*
C13	*Hinged NiTiCon*	*Nitinol rod*	*Heat shrink*
C14	*Nitinol rod*	*Inner axis shaft*	*Heat shrink*
C15	*Nitinol rod*	*PEEK overtube*	*Adhesive*
C16	*Tip base revised*	*Overtube*	*Welding*

B) FEM reports

FEM - 1

Simulation 1

Title:	**FEM-1 | PEEK base and Lower jaw + Connector bolt**
Author:	Philip de Haes
Details:	Component No: 2 | 3 | 8 Part-file name: PH_4001_v8 – PEEK base Part-file name: PH_4002_v8 – Lower Jaw Assembly CAD-file name: FEM-1 – Sep – 15 20mm jaw Study name: Static 1 Date: 15-09-2020
Summary:	The most important questions are: Is the bolt connection between the two components strong enough to withstand the applied force? Is the PEEK component stiff enough to withstand the uniformly distributed load of 20N on the lower jaw's seal surface? The bolt connection has a safety factor of 2.8 calculated by Solidworks in the simulation. From this it is concluded that the bolt diameter, length and pre-load are sufficient. The connection between the two components is thus sufficient. The PEEK component will show stresses close to yield. A fatigue test can determine whether the PEEK component is actually strong enough. Side note, 2 more stainless steel conductor rods are slid through the PEEK part in reality, which can provide extra rigidity. It is extremely important that a reinforced PEEK is chosen, for example glass-fiber reinforced PEEK. (Carbon fiber PEEK conducts electricity and does not comply).
Assumptions:	- Both the conductor rods where excluded from this simulation. - An ideal uniformly distributed compression force of 20N is applied on the surface of the lower jaw. - The contact set(s) between the two components are set to: No penetration with a friction coefficient of 0.3. Although in reality the contacting surfaces will be bonded with adhesives to prevent gap forming.
Study details:	Analysis type: Static Mesh type: Solid Mesh Solver type: FFEPlus (Solidworks default) Large displacement: off Length/Displacement: mm Temperature: Celsius Angular velocity: Rad/sec Pressure/Stress: MPa

Model Information

Model:	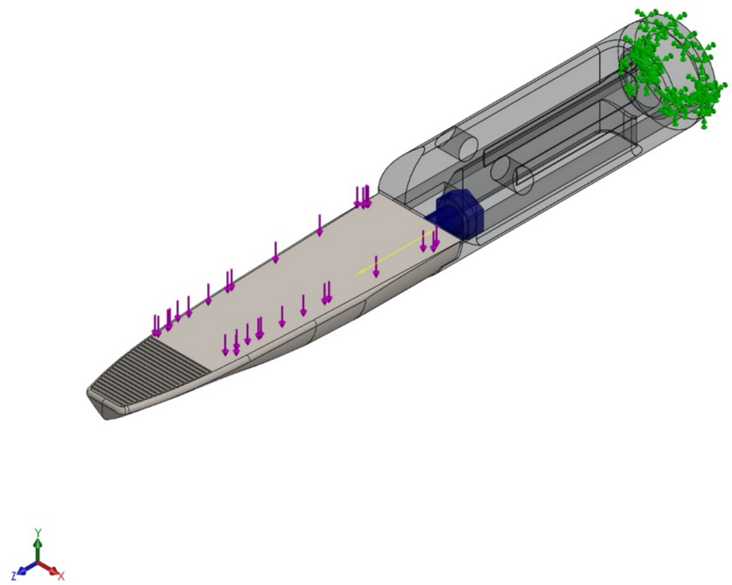	
Solid bodies properties:	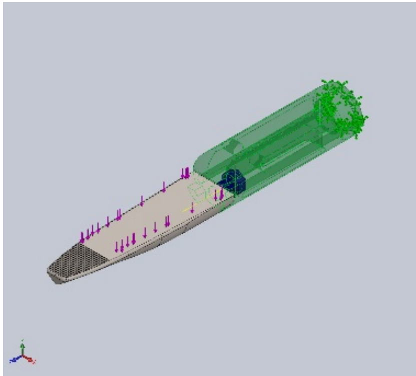	**Mass: 0,000282757 kg** **Volume: 1,8481e-07 m^3** **Density: 1.529,99 kg/m^3** **Weight: 0,00277101 N**
	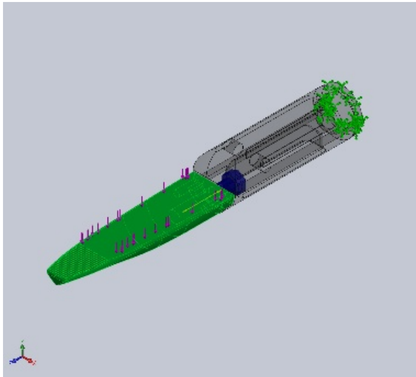	**Mass: 0,00106567 kg** **Volume: 1,32761e-07 m^3** **Density: 8.027,04 kg/m^3** **Weight: 0,0104436 N**
Material Properties:	Component **2** Name: **KetaSpire KT-820 GF30 BK95** Model type: **Linear Elastic Isotropic** Default failure criterion: **Unknown** Yield strength: **158 N/mm^2** Tensile strength: **158 N/mm^2** Compressive strength: **169 N/mm^2** Elastic modulus: **10.500 N/mm^2** Poisson's ratio: **0,34**	Component **3** Name: **AISI Type 316L stainless steel** Model type: **Linear Elastic Isotropic** Default failure criterion: **Max von Mises Stress** Yield strength: **170 N/mm^2** Tensile strength: **485 N/mm^2** Elastic modulus: **200.000 N/mm^2** Poisson's ratio: **0,265** Mass density: **8,027 g/cm^3**

	Mass density: **1,53 g/cm^3** Shear modulus: **318,9 N/mm^2**	Shear modulus: **82.000 N/mm^2** Thermal expansion coefficient: **1,65e-05 /Kelvin**

Loads and Fixtures

Fixture:	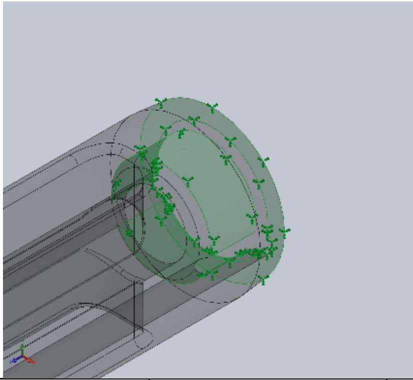	Entities: **4 face(s)** Type: **Fixed Geometry**

Resultant forces:	Components	X	Y	Z	Resultant
	Reaction Force (N)	-2,08616e-07	20	-1,48416e-05	20
	Reaction Moment (N*m)	0	0	0	1e-33

Load:	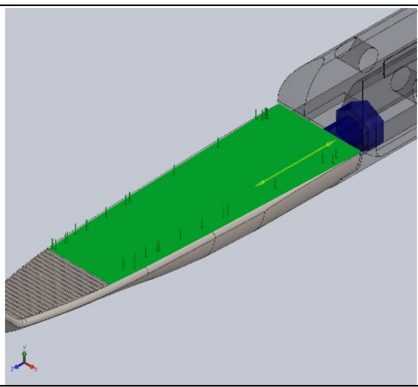	Entities: **1 face(s)** Type: **Apply normal force** Value: **20 N**

Connector Definitions

Connector details:	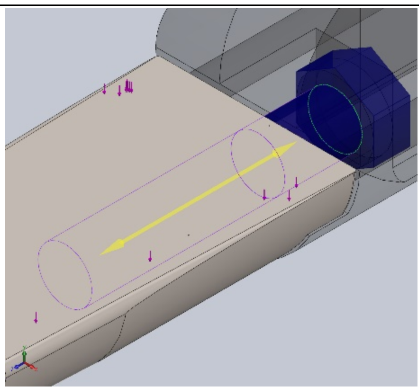	Entities: **1 edge(s), 2 face(s)** Type: **Bolt(Head/Nut diameter)(Counterbore screw)** Head diameter: **2 mm** Nominal shank diameter: **1,4 mm** Preload (Axial): **200** Young's modulus: **2e+11** Poisson's ratio: **0,265**	**Strength details:** Bolt Check: **OK** Calculated FoS: **2,82677** Desired FoS: **2** 

	Type	X	Y	Z	Resultant

Connector Forces:	Axial Force (N)	0	0	-200	200
	Shear Force (N)	0,00082981	-0,00098098	0	0,0012849
	Bending moment (N*m)	-3,8716e-06	2,0514e-06	0	4,3815e-06

Contact information

Contact set:	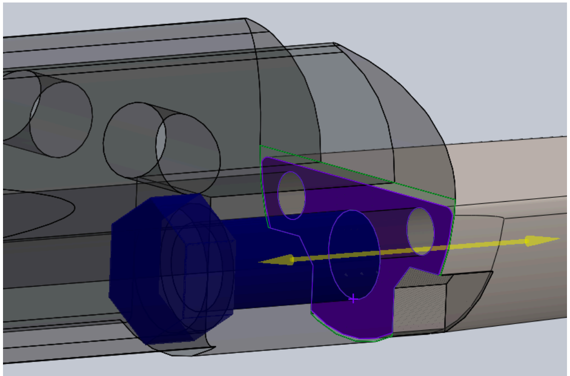	Type: **No Penetration contact pair** Entities: **2 face(s)** Friction Value: **0,3** Advanced: **Node to surface** ***Entities: All remaining contact faces are set to No Penetration***

Contact/Friction force:	Components	X	Y	Z	Resultant
	Contact Force (N)	**0**	**0**	**-7,9244**	**7,9244**
	Friction Force (N)	**-0,035392**	**-0,47293**	**5,9985E-19**	**0,47425**

Mesh Details

Mesh:	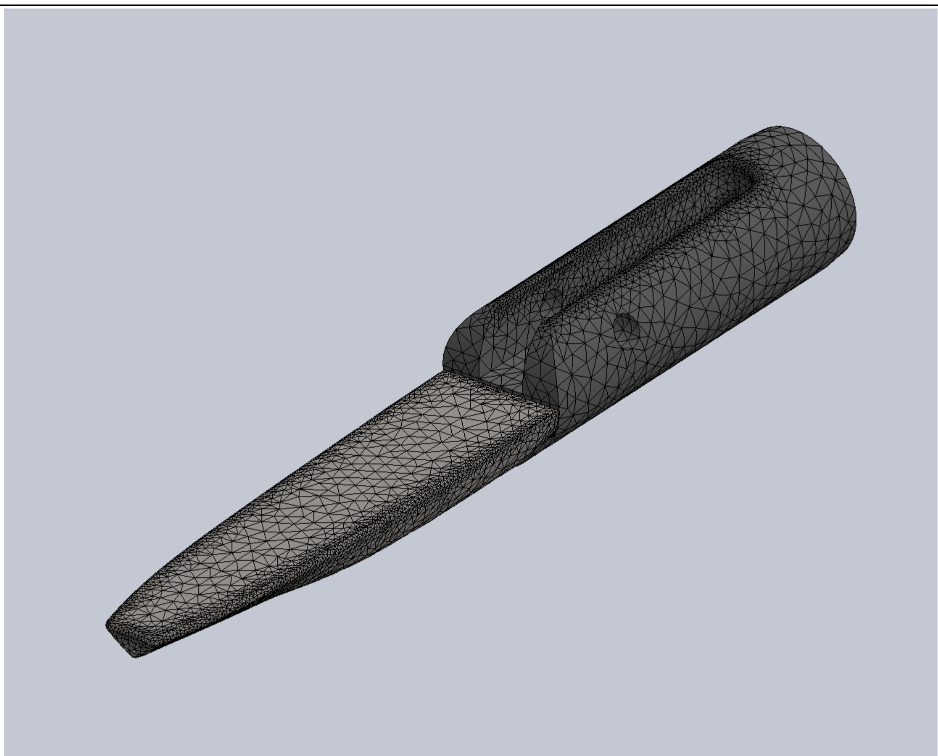	
Mesh information: **Mesh control:**	Mesh type: **Solid mesh** Mesher used: **Curvature-based mesh** Jacobian points: **4** Max element size: **0,680496mm** Min element size: **0,136099 mm** Mesh Quality: **High** Total nodes: **103132** Total elements: **63652**	Entities: **1 face(s)** Units: **mm** Size: **0,160866** Ratio: **0,160866**

Resultant Forces

Reaction forces:	Selection set	Units	Sum Xs	Sum Y	Sum Z	Resultant
	Entire model	**N**	**-2,08616e-07**	**20**	**-1,48416e-05**	**20**

Study Results

VON: von Mises Stress	Min: 0,0 N/mm^2 (MPa) Node: 76741	Max: 207,9 N/mm^2 (MPa) Node: 74403
Picture(s)	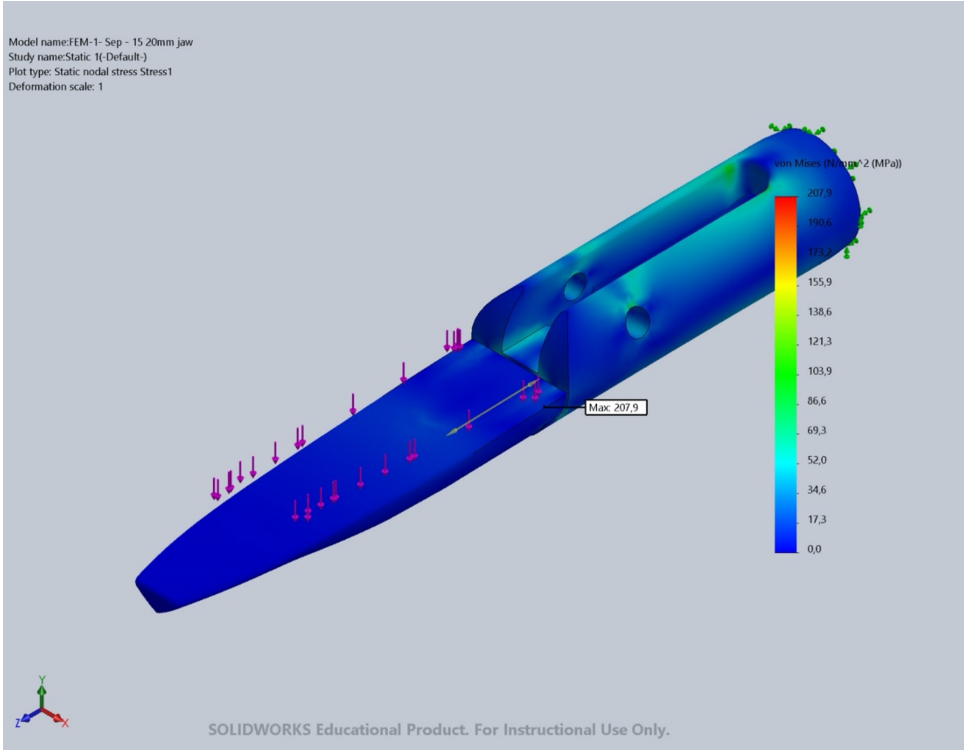	
Discussion:	The highest stresses are above yield, however they are considered as ‘stress concentrations’ or ‘stress singularities’ and most likely do not cause the materials to yield. They are pointed out and discussed in the sections below.	
URES: Resultant Displacement	Min: 0,000e+00 mm Node: 25	Max: 8,677e-01 mm Node: 73577

Picture(s)	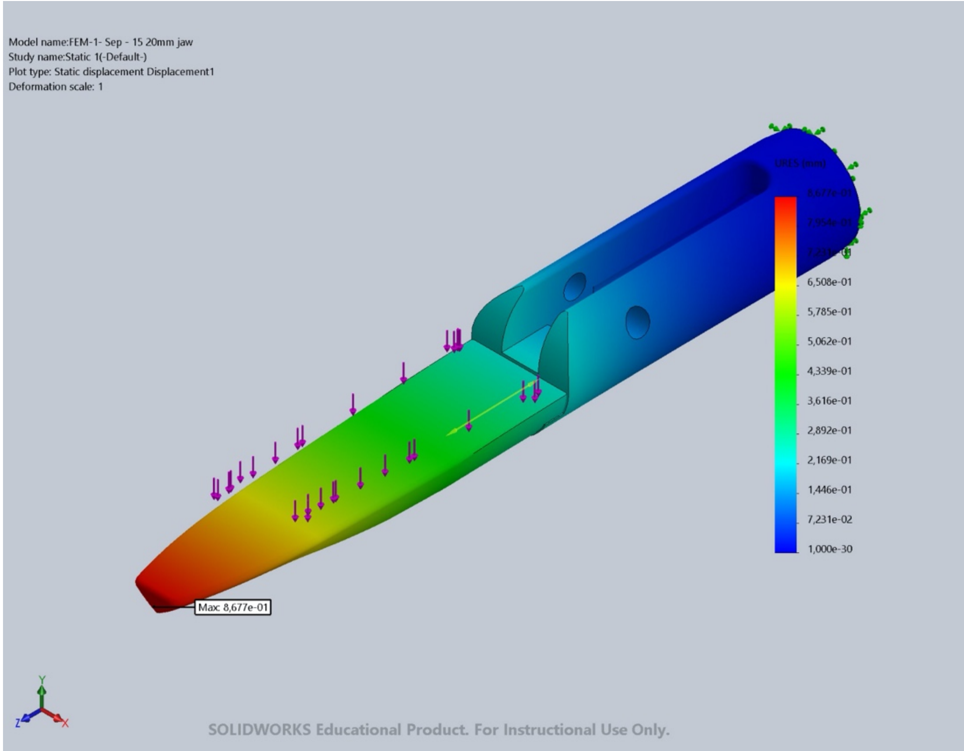	
Discussion:	Max displacement is acceptable. This is considered as first indication that the model does not yield due to the high stresses.	
ESTRN: Equivalent Strain	Min: 5,688e-10 Element: 57343	Max: 8,567e-03 Element: 31556
Picture(s)	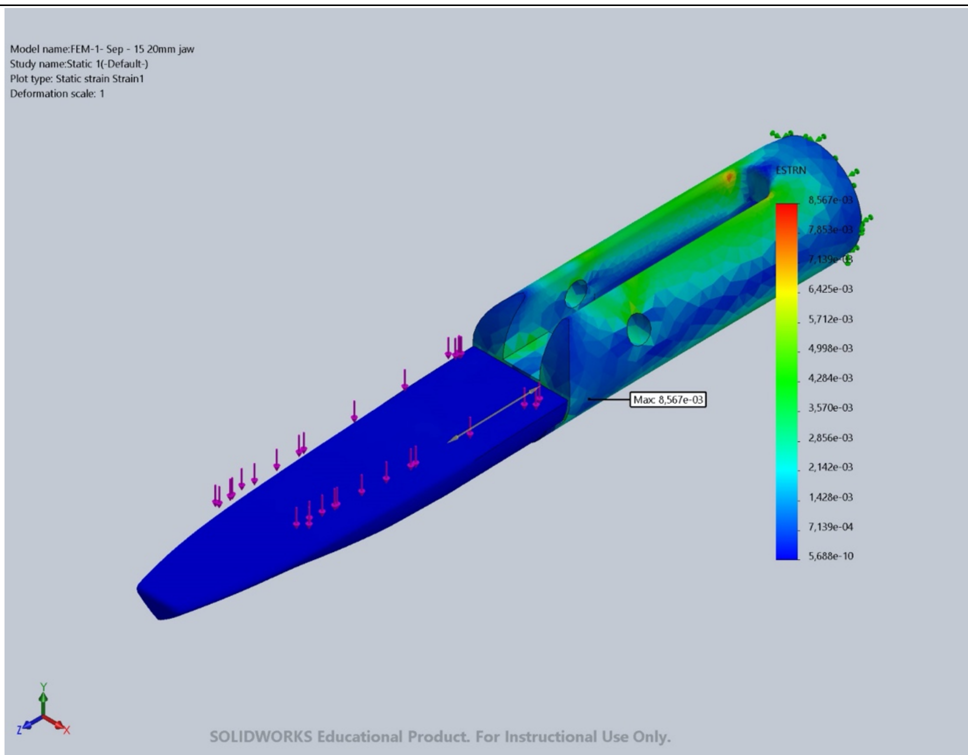	
Discussion:	Max strain is very low.	
Factor of Safety	Min: 1,38 Node: 26579	Max: 3.077,96 Node: 11512

Picture(s)	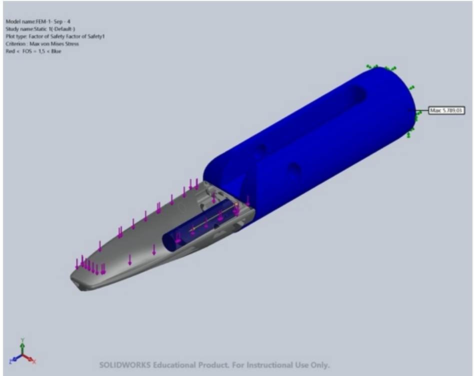
Discussion:	Red areas: FoS <1.5. Sharp edges consisting of stress concentrations cause the safety factor to be below 1.5 in these areas.
Factor of Safety	Min: 0,82 Node: 74403 — Max: 1.692.671,00 Node: 76741
Picture(s)	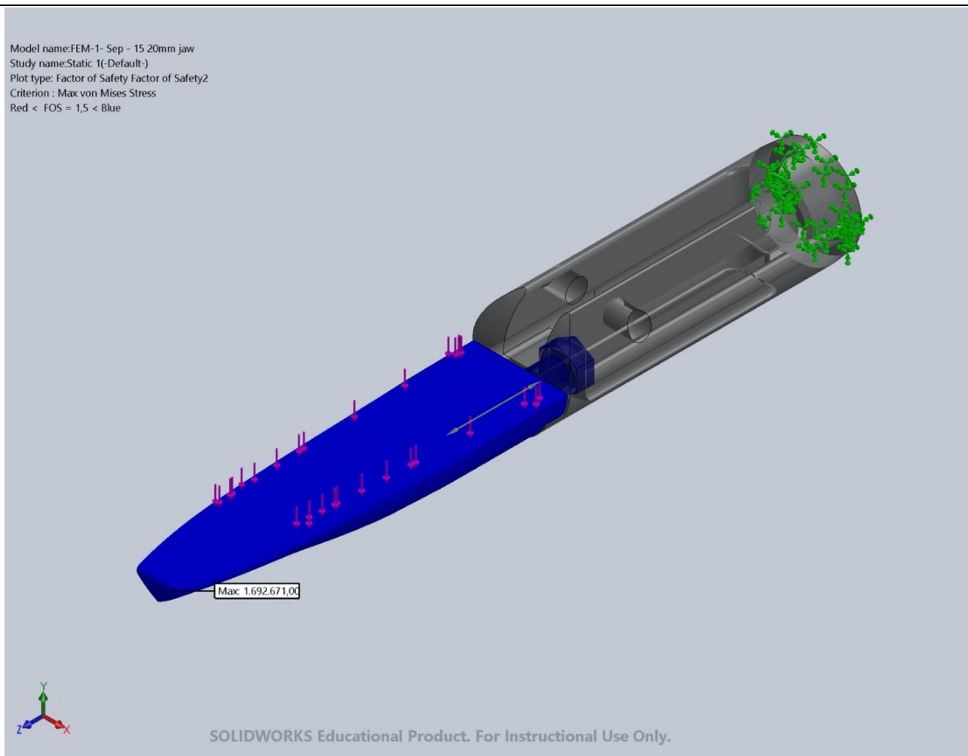
Discussion:	Red areas: FoS <1.5. Due to high stress concentrations the safety factor cannot be trusted. Stress concentrations are discussed below.
VON: von Mises Stress Component:	Min: 0,0 N/mm^2 (MPa) Node: 76741 — Max: 114,2 N/mm^2 (MPa) Node: /

Picture(s)	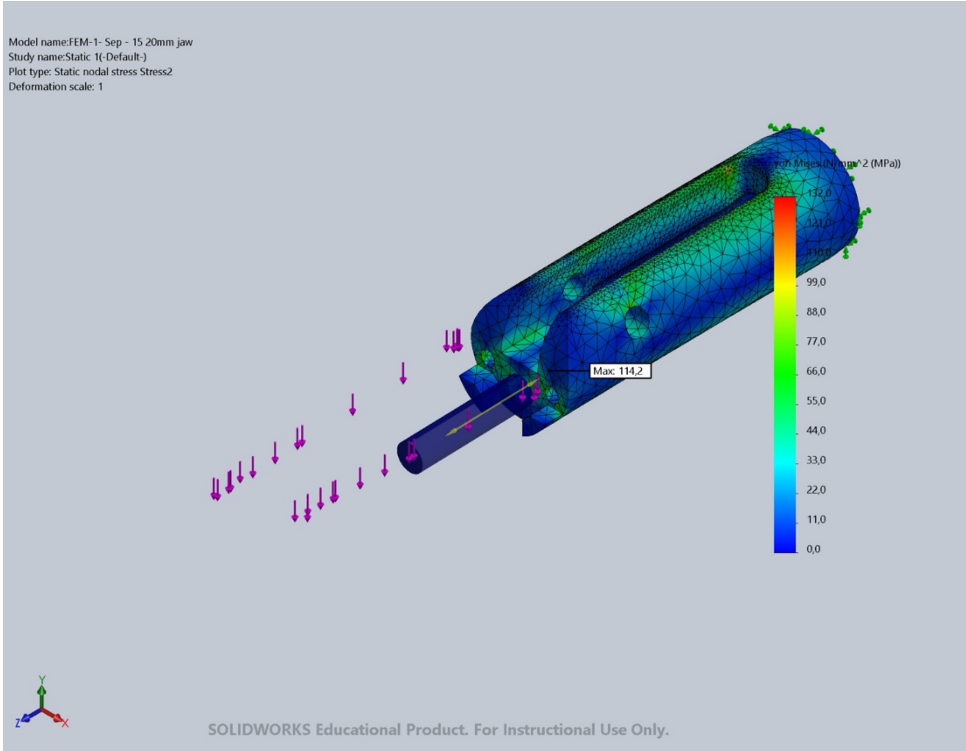
Discussion:	Maximum stress is 114.2 MPa. The safety factor in this stress areas is below 1.5, however the stresses are still below yield strength.
	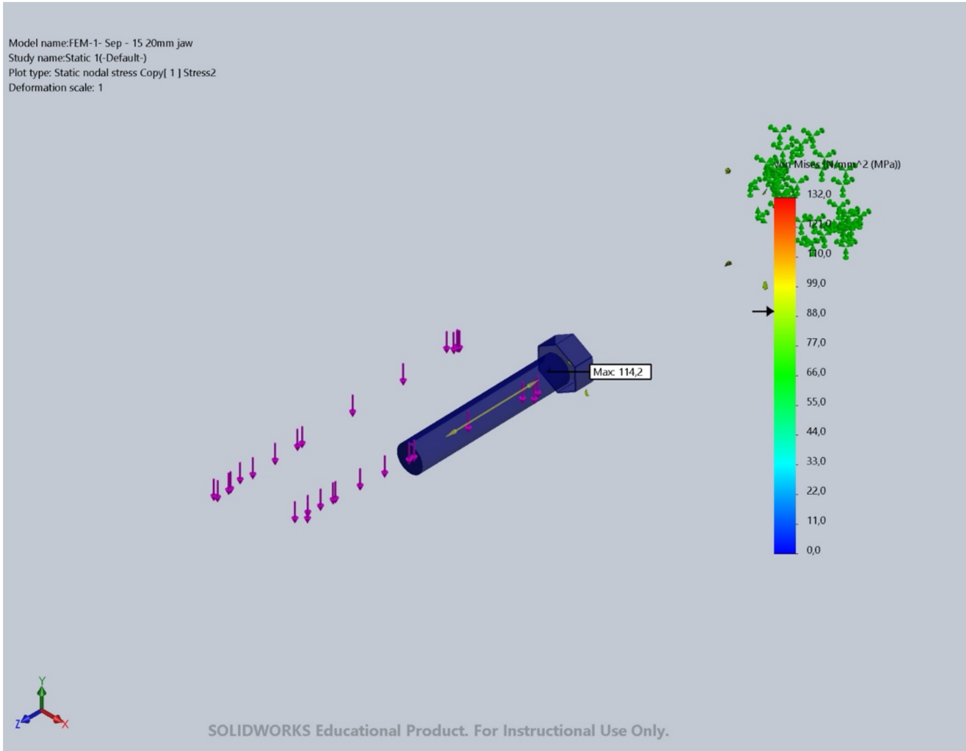
Discussion:	ISO clipping plot shows stress area >90 MPa. They indicate
VON: von Mises Stress Component:	Min: 0,0 N/mm^2 (MPa) Node: 76741 Max: 207,9 N/mm^2 (MPa) Node: 74403

Picture(s)	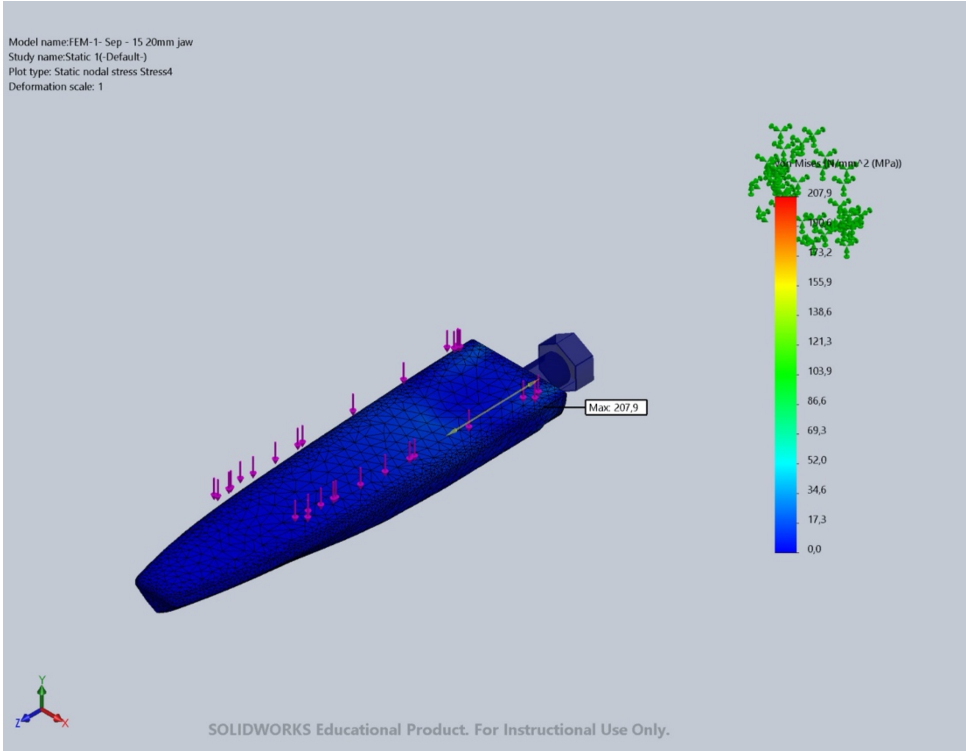
Discussion:	
	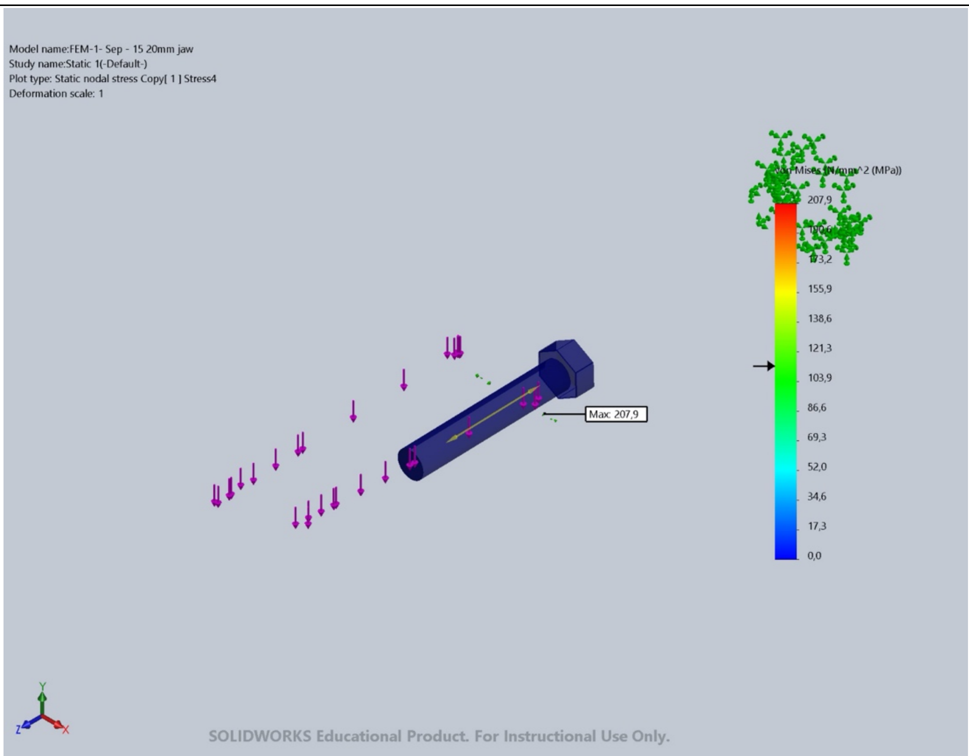
Discussion:	ISO clipping plot shows stress area >113MPa. As can be seen, small parts of the top layer of elements show high stress concentrations.

<table>
<tr><td>Additional information</td><td>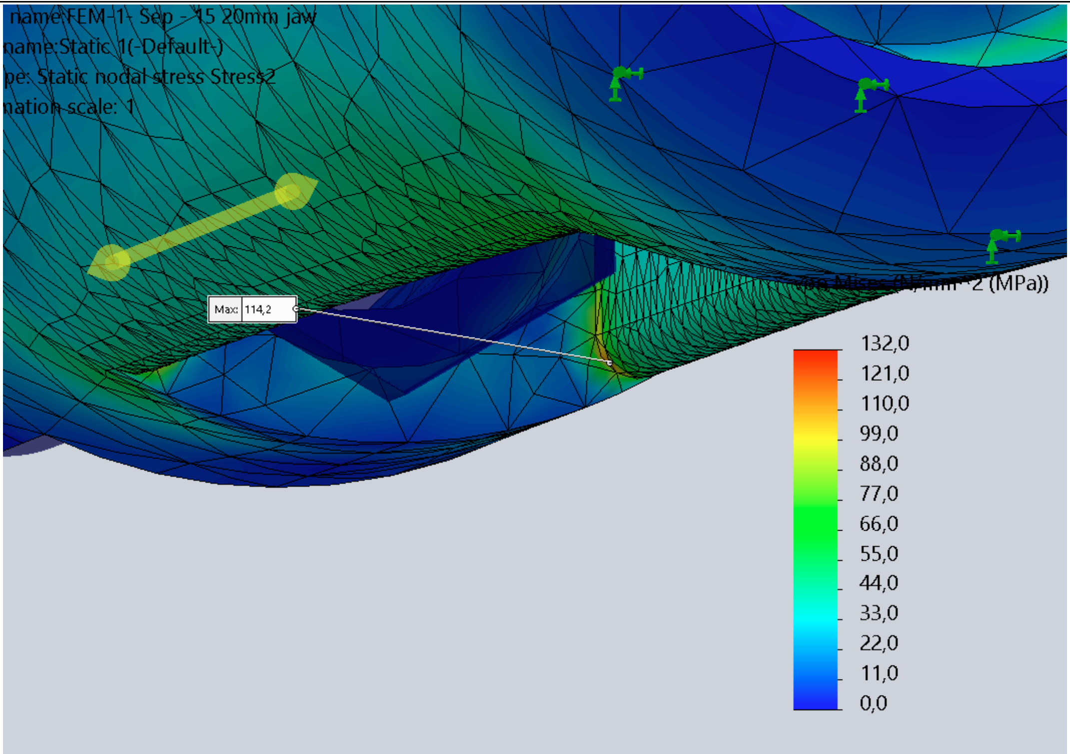
</td></tr>
<tr><td>Discussion:</td><td>Highest stress occurs near all 4 of these ‘sharp’ edges in the PEEK base component.</td></tr>
<tr><td></td><td></td></tr>
<tr><td>Additional information</td><td>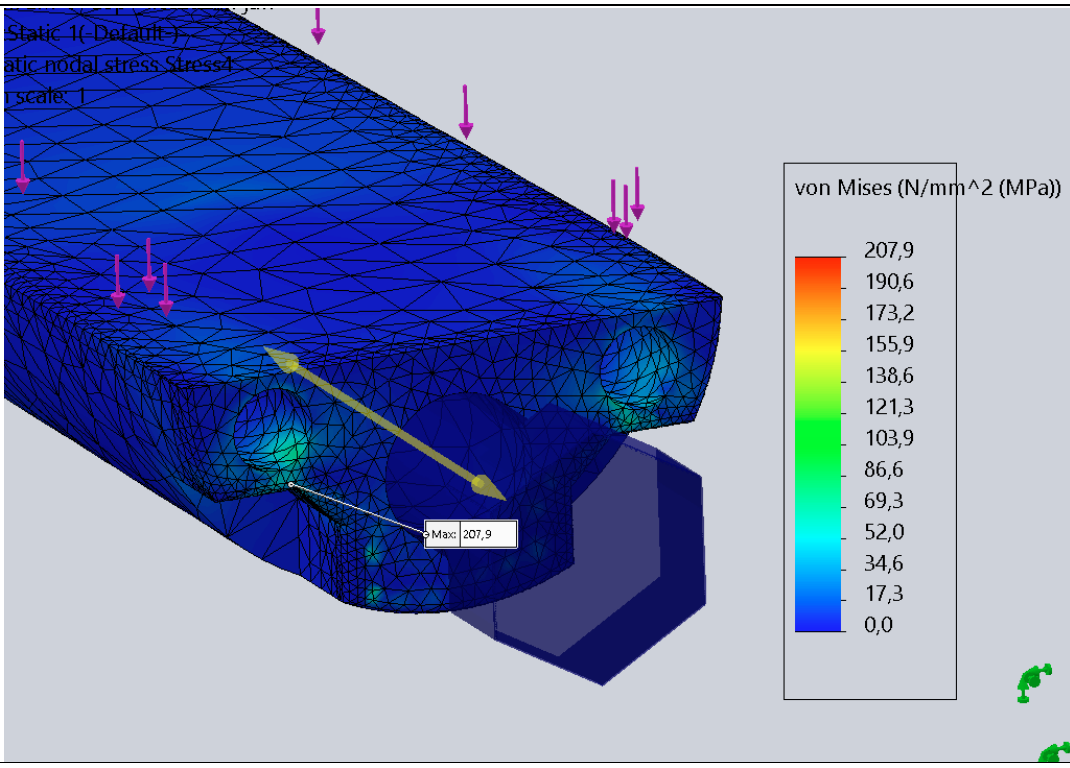
</td></tr>
<tr><td>Discussion:</td><td>Close-up of the stress areas above yield strength.</td></tr>
<tr><td></td><td></td></tr>
</table>

Additional information	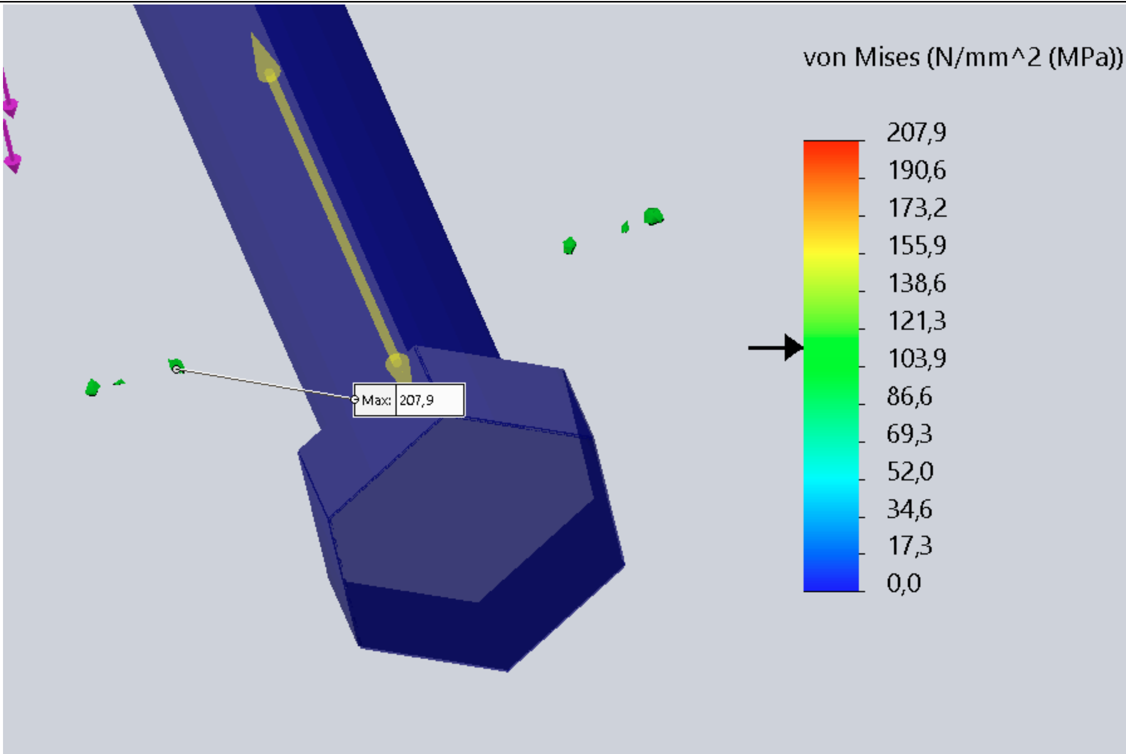
Discussion:	ISO plot shows that only the green coloured (tiny) areas show high stresses. It is very unlikely that these will cause the component to fail due to fatigue.

Study Conclusion

Conclusion:	The stress at some distance from the stress concentrations are trusted, i.e. stresses in the second row of elements behind the stress concentrations. In this case, the stresses are acceptable for the lower jaw component. This is also underlined by the displacement and strain plots. Stress concentrations in the lower jaw component are unlikely to cause fatigue. Fatigue tests must be conducted to determine the lifespan of the PEEK component. A glass fiber reinforced PEEK material must be chosen. However, it must also be considered that in reality the PEEK component will be reinforced by two metal conductor rods. The bolt connection has a FoS of 2.8 and appears to be a viable solution for connecting the two components. Based on FEM-1 simulation, a uniformly distributed pressure of 20N can be applied to the Lower jaw without damaging the connection between the Lower jaw and PEEK base.

FEM - 2

Simulation 2

Title:	**FEM-2 | Upper jaw**
Author:	Philip de Haes
Details:	Component No: **4** Part-file name: PH_4003_v8 – Upper Jaw CAD-file name: FEM-2 - Sep – 15 – 20mm Jaw Study name: Static 2 L1 = 9_95 mm Date: 15-09-2020
Summary:	This simulation is based on the maximum tensile force (55 N) that will be applied to this component, regarding the required sealing pressure. Higher stresses occur surrounding the hinge axis holes, where the connector component is attached. These stresses are occurring in the first layer of elements and do not radiate deeper into the material. Future fatigue tests should be done to evaluate the stresses near the arched surface.
Assumptions:	For this simulation it is assumed that the instrument jaw is in a fully closed configuration. Therefore a constraint in y-direction (i.e. normal to part of the sealing surface of the Upper jaw) has been applied (Slider / Roller). Two rigid hinges axes are applied. The upper rigid hinge axis is constraint with a ‘fixed hinge’, that is the jaw’s axis of rotation. The lower rigid hinge axis has a force (55 N) applied to its face.
Study details:	Analysis type: Static Mesh type: Mixed Mesh Solver type: FFEPlus (Solidworks default) Large displacement: off
	Length/Displacement: mm Temperature: Celsius Angular velocity: Rad/sec Pressure/Stress: MPa

Model Information

Model:	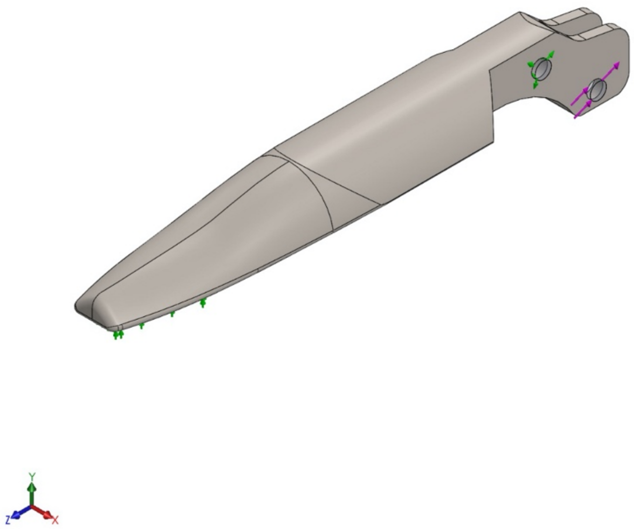

Solid bodies properties:	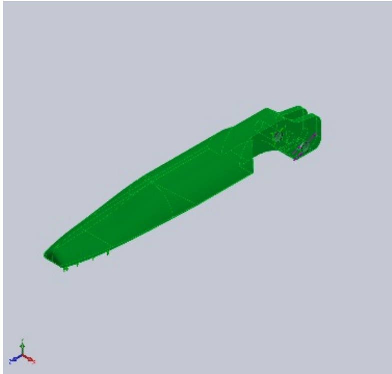	**Mass: 0,00144055 kg** **Volume: 1,79458e-07 m^3** **Density: 8.027,24 kg/m^3** **Weight: 0,0141174 N**
Material Properties:	Name: **AISI Type 316L stainless steel** Model type: **Linear Elastic Isotropic** Default failure criterion: **Max von Mises Stress** Yield strength: **170 N/mm^2** Tensile strength: **485 N/mm^2** Elastic modulus: **200.000 N/mm^2** Poisson's ratio: **0,265** Mass density: **8,027 g/cm^3** Shear modulus: **82.000 N/mm^2** Thermal expansion coefficient: **1,65e-05 /Kelvin**	

Loads and Fixtures

Fixture:	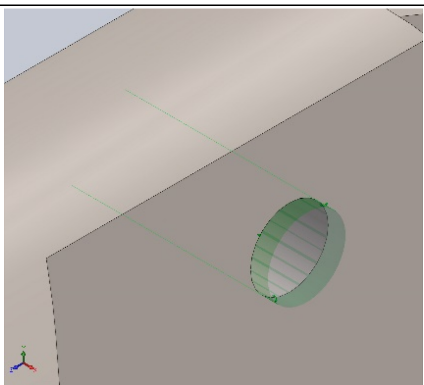		Entities: **1 face(s)** Type: **Fixed Hinge**		
Resultant forces:	Components	X	Y	Z	Resultant
	Reaction Force (N)	**0**	**0**	**0**	**1e-33**
	Reaction Moment (N*m)	**0**	**0**	**0**	**1e-33**
Fixture:	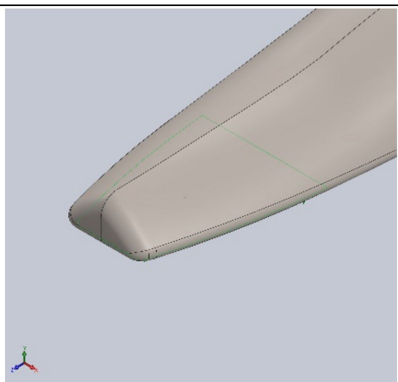		Entities: **1 face(s)** Type: **Roller/Slider**		
Resultant forces:	Components	X	Y	Z	Resultant
	Reaction Force (N)	2,11752e-06	12,3828	-6,7683e-06	12,3828

	Reaction Moment (N*m)	0	0	0	1e-33

Load:	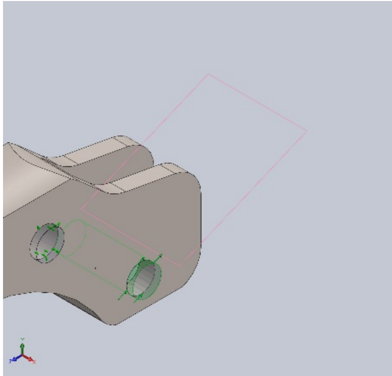	Entities: **1 face(s), 1 plane(s)** Reference: **Plane2** Type: **Apply force** Values: **55; ---; --- N** Moments: **---; ---; --- N.m**

Contact information

Contact set 1:	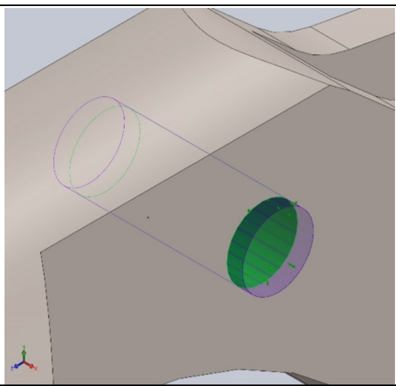			Type: **No Penetration contact pair** Entities: **2 face(s)** Advanced: **Node to surface**	
Contact/Friction force:	Components	X	Y	Z	Resultant
	Contact Force (N)	**2,0708E-17**	**1,6889E-14**	**5,2851E-13**	**5,2878E-13**
Contact set 2:	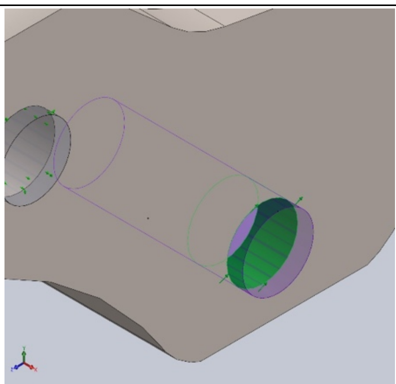			Type: **No Penetration contact pair** Entities: **2 face(s)** Advanced: **Node to surface**	
Contact/Friction force:	Components	X	Y	Z	Resultant
	Contact Force (N)	**0,0062712**	**-10,652**	**25,357**	**27,503**

Contact set 2:	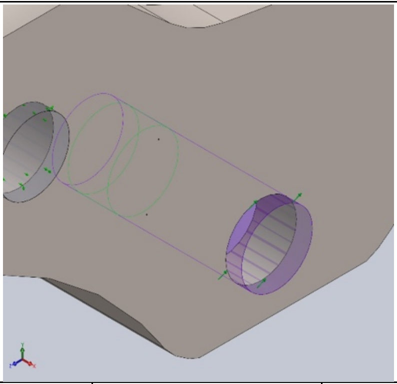		Type: **No Penetration contact pair** Entities: **2 face(s)** Advanced: **Node to surface**		
Contact/Friction force:	Components	X	Y	Z	Resultant
	Contact Force (N)	**-0,0062678**	**-10,658**	**25,346**	**27,496**

Mesh Details

Mesh information:	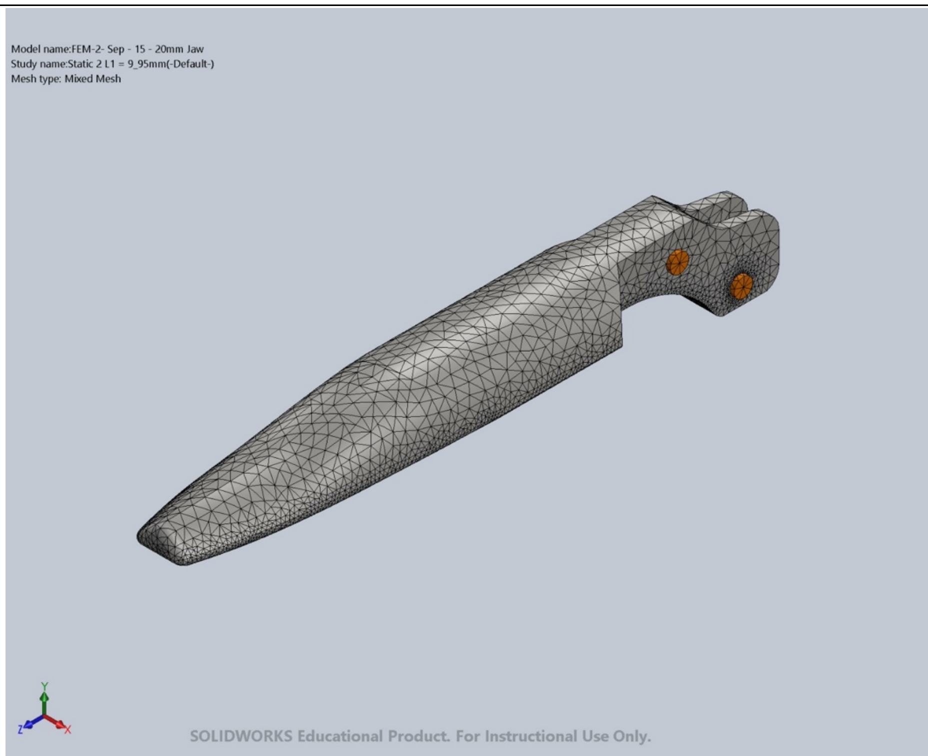	
Mesh information: **Mesh Control:**	Mesh type: **Mixed mesh** Mesher used: **Curvature-based mesh** Jacobian points: **4** Max element size: **0,564312 mm** Min element size: **0,112862 mm** Mesh Quality: **High** Total nodes: **65345** Total elements: **40553**	Entities: **3 face(s)** Units: **mm** Size: **0,141086** Ratio: **0,141086**

Resultant Forces

Reaction forces:	Selection set	Units	Sum X	Sum Y	Sum Z	Resultant
	Entire model	**N**	**2,11752e-06**	**12,3828**	**-6,7683e-06**	**12,3828**
	Incorrect values due to use of rigid bodies in simulation. The force is applied on one of the rigid bodies.					

Study Results

<table>
<tr><td>VON: von Mises Stress</td><td>Min: 0,0 N/mm^2 (MPa)
Node: 64706</td><td>Max: 154,0 N/mm^2 (MPa)
Node: 437</td></tr>
<tr><td>Picture(s)</td><td colspan="2">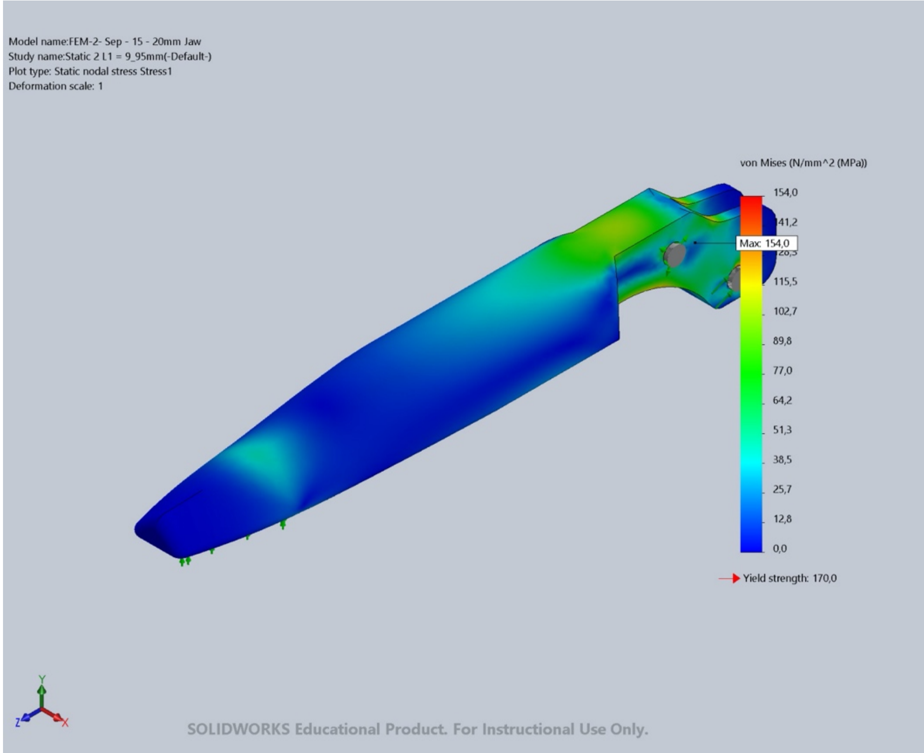
</td></tr>
<tr><td>Discussion:</td><td colspan="2"></td></tr>
<tr><td></td><td colspan="2"></td></tr>
<tr><td>URES: Resultant Displacement</td><td>Min: 2,515e-10 mm
Node: 65111</td><td>Max: 1,807e-02 mm
Node: 450</td></tr>
<tr><td>Picture(s)</td><td colspan="2">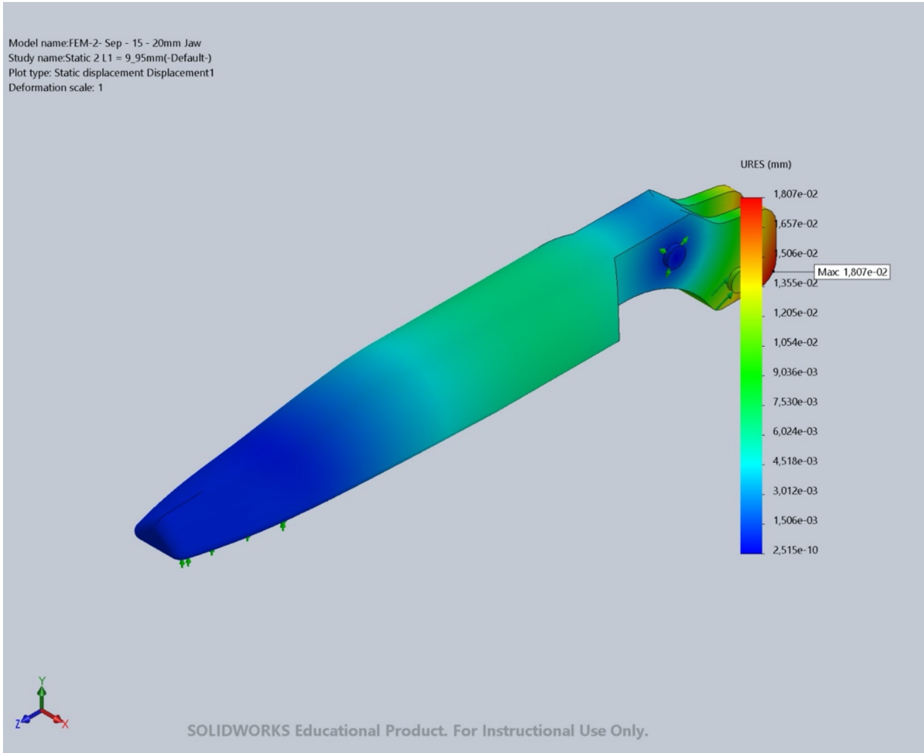
</td></tr>
<tr><td>Discussion:</td><td colspan="2">Max displacement is acceptable.</td></tr>
<tr><td>ESTRN: Equivalent Strain</td><td>Min: 0,000e+00
Element: 40236</td><td>Max: 6,187e-04
Element: 11945</td></tr>
</table>

<table>
<tr><td>Picture(s)</td><td colspan="2">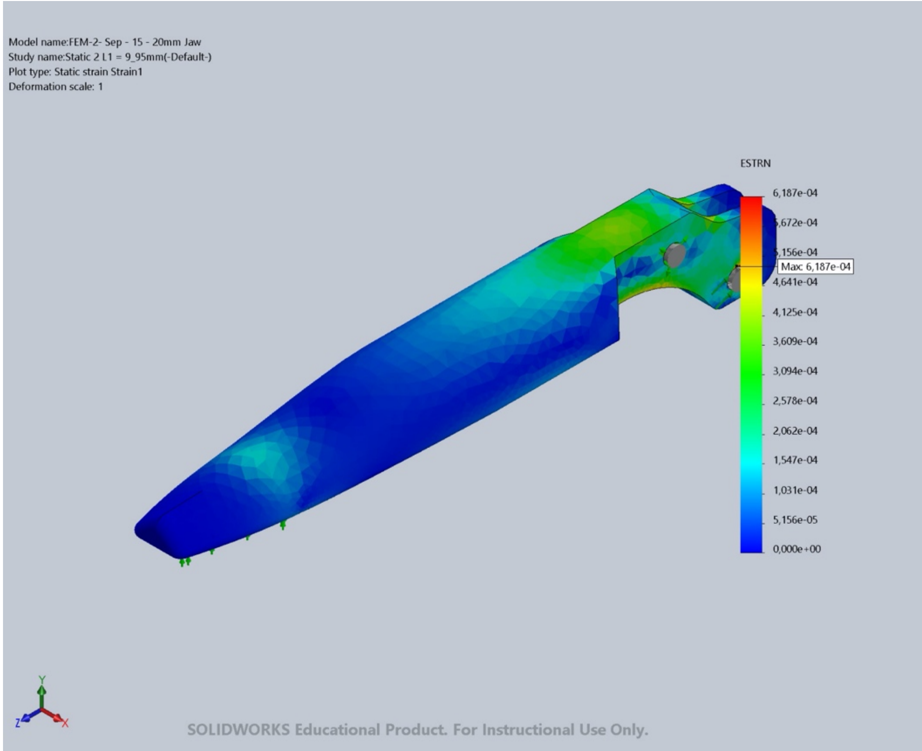
</td></tr>
<tr><td>Discussion:</td><td colspan="2">Negligible strain. Indication that the model probably does not yield.</td></tr>
<tr><td>Factor of Safety</td><td>Min: 1,10
Node: 437</td><td>Max: 245.213,28
Node: 24883</td></tr>
<tr><td>Picture(s)</td><td colspan="2">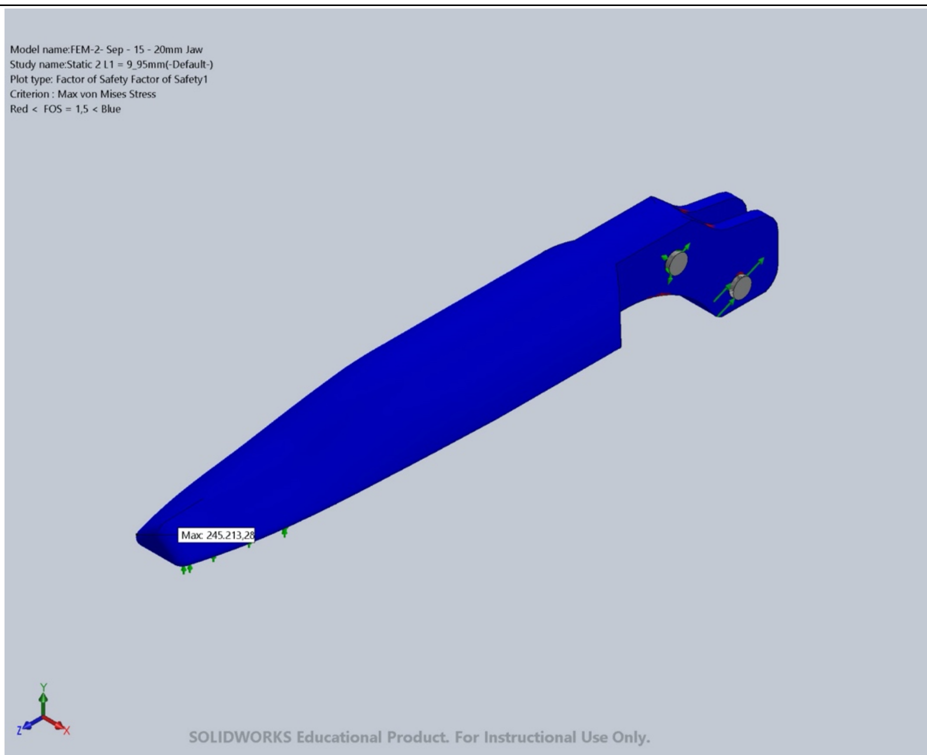
</td></tr>
<tr><td>Discussion:</td><td colspan="2">Red areas: FoS <1.5. Critical areas are illustrated in red.</td></tr>
<tr><td></td><td colspan="2"></td></tr>
</table>

<table>
<tr><td>Additional information</td><td>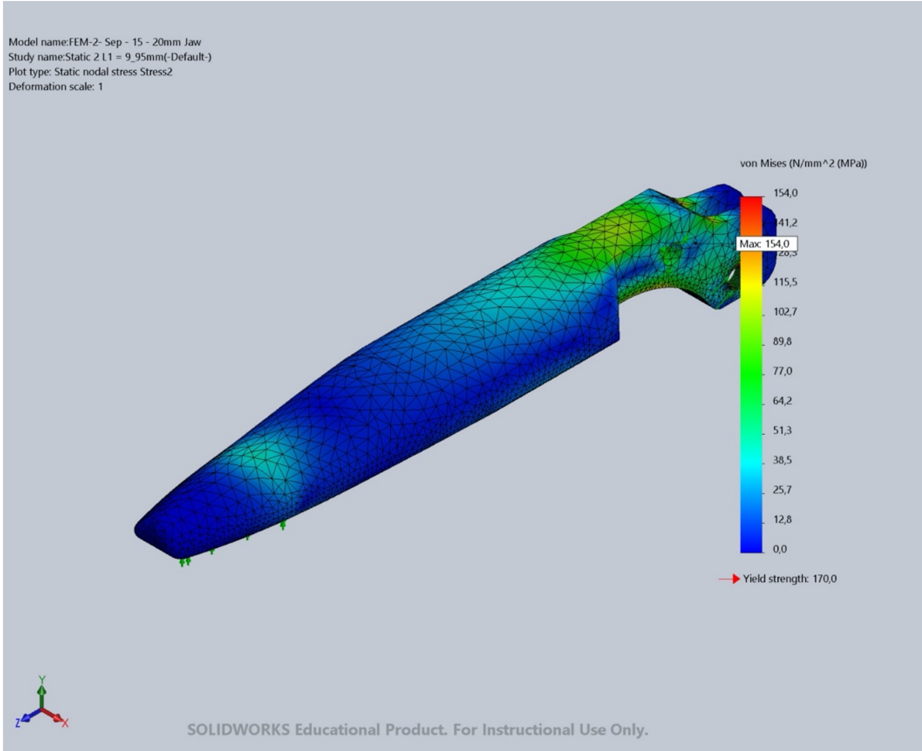
</td></tr>
<tr><td>Discussion:</td><td>In this figure the elements and their stresses are illustrated. High stresses occurred around the holes in the first layer of elements and below the arch. Stress levels are just 15 MPa below yield strength. Fatigue test should be done.</td></tr>
<tr><td></td><td></td></tr>
<tr><td>Additional information</td><td>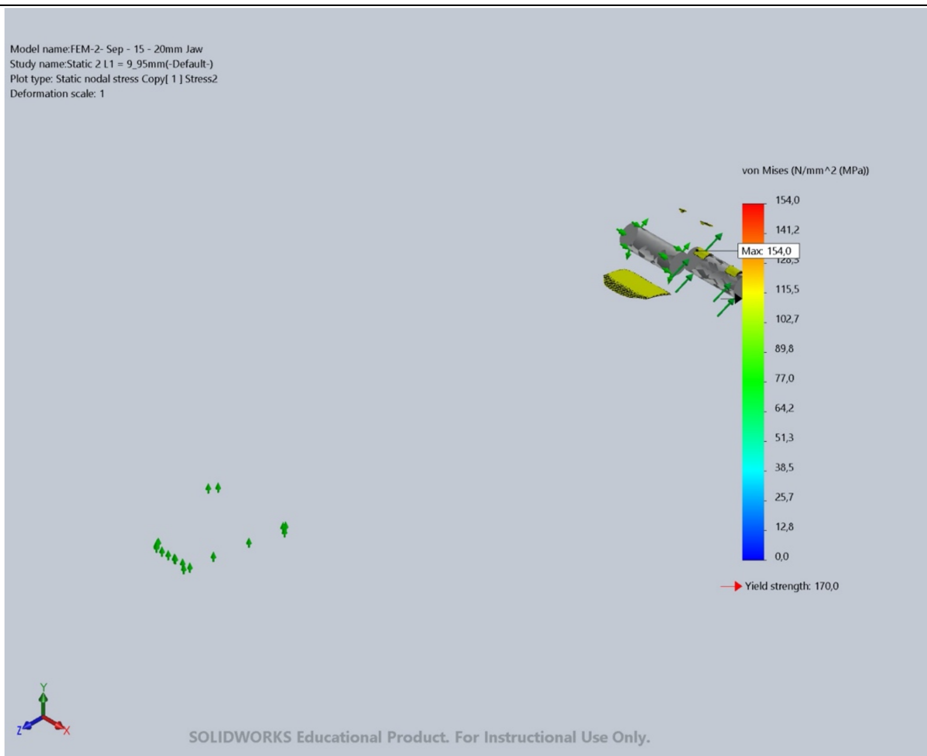
</td></tr>
<tr><td>Discussion:</td><td>ISO clipping plot shows stress area >113 MPa, thus areas with a safety factor <1.5. Indicates critical stresses occur only around the holes near the surface.</td></tr>
<tr><td></td><td></td></tr>
</table>

Study Conclusion

Conclusion:	Higher stresses occur surrounding the hinge axis holes, where the connector component is attached. These stresses are occurring in the first layer of elements and do not radiate deeper into the material. Future fatigue tests should be done to evaluate the stresses near the arched surface.

FEM - 3

Simulation 3

Title:	**FEM-3 | Connector**
Author:	Philip de Haes
Details:	Component No: **5** Part-file name: PH_4004_v8 – Connector CAD-file name: FEM -3 – Sep – 15 Study name: Static 2 L1 = 9_95 mm Date: 15-09-2020
Summary:	This simulation is based on the maximum tensile force (55N) that will be applied to this component, regarding the required sealing pressure. From this simulation it can be concluded that this component has a correct design since the safety factor of >1.5 applies to most of the component.
Assumptions:	The Connector component links the Upper jaw (4) with the NiTiCon (6) component and has two hinge connections. On both ends a rigid hinge axis is placed. One rigid axis is constraint with a 'fixed hinge', the other rigid axis has a force (55N) applied.
Study details:	Analysis type: Static Mesh type: Mixed Mesh Solver type: FFEPlus (Solidworks default) Large displacement: off Length/Displacement: mm Temperature: Celsius Angular velocity: Rad/sec Pressure/Stress: MPa

Model Information

Model:	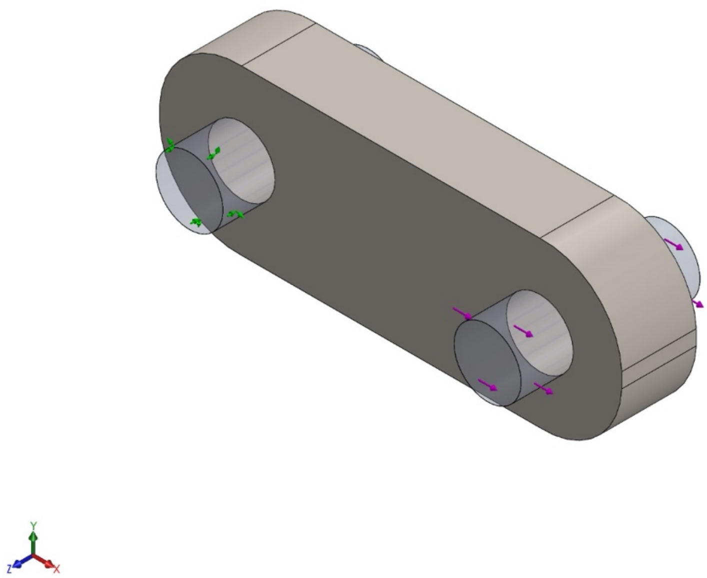

Solid bodies properties:	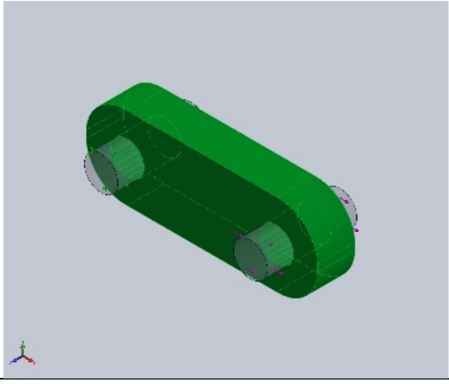	Mass: **9,17415e-05 kg** Volume: **1,14291e-08 m^3** Density: **8.027 kg/m^3** Weight: **0,000899067 N**
Material Properties:	Name: **AISI Type 316L stainless steel** Model type: **Linear Elastic Isotropic** Default failure criterion: **Max von Mises Stress** Yield strength: **170 N/mm^2** Tensile strength: **485 N/mm^2** Elastic modulus: **200.000 N/mm^2** Poisson's ratio: **0,265** Mass density: **8,027 g/cm^3** Shear modulus: **82.000 N/mm^2** Thermal expansion coefficient: **1,65e-05 /Kelvin**	

Loads and Fixtures

Fixture:	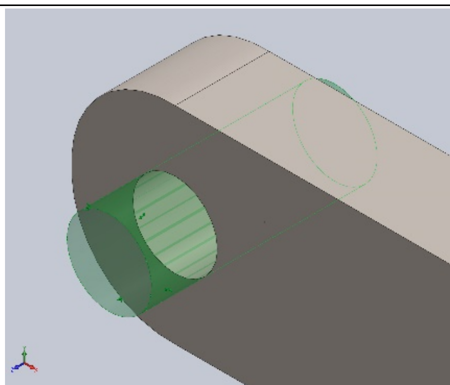		Entities: **1 face(s)** Type: **Fixed Hinge**		
Resultant forces:	Components	X	Y	Z	Resultant
	Reaction Force (N)	**0**	**0**	**0**	**1e-33**
	Reaction Moment (N*m)	**0**	**0**	**0**	**1e-33**
Load:	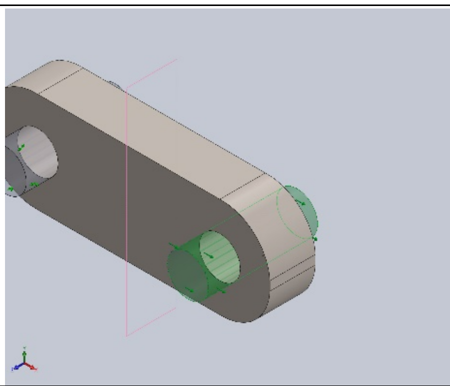		Entities: **1 face(s), 1 plane(s)** Reference: **Right Plane** Type: **Apply force** Values: **---; ---; 55 N** Moments: **---; ---; --- N.m** ***The force is directed along the longitudinal axis of the connector component.***		

Contact information

Contact set 1:	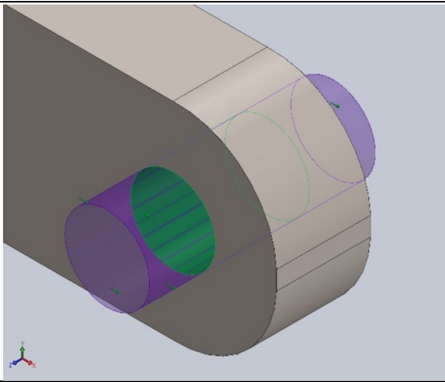			Type: **No Penetration contact pair** Entities: **2 face(s)** Advanced: **Node to surface**	
Contact/Friction force:	Components	X	Y	Z	Resultant
	Contact Force (N)	**-1,7173E-13**	**-6,2284E-14**	**6,7233E-19**	**1,8268E-13**
Contact set 2:	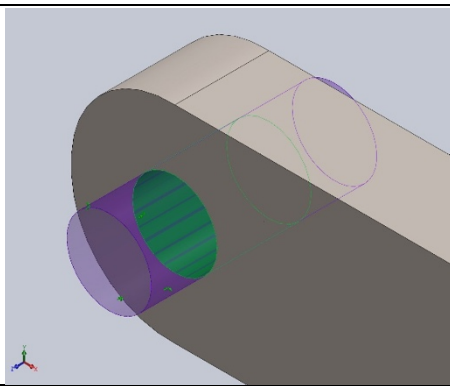			Type: **No Penetration contact pair** Entities: **2 face(s)** Advanced: **Node to surface**	
Contact/Friction force:	Components	X	Y	Z	Resultant
	Contact Force (N)	**6,9153E-13**	**-4,4274E-14**	**-1,0057E-18**	**6,9295E-13**

Mesh Details

Mesh	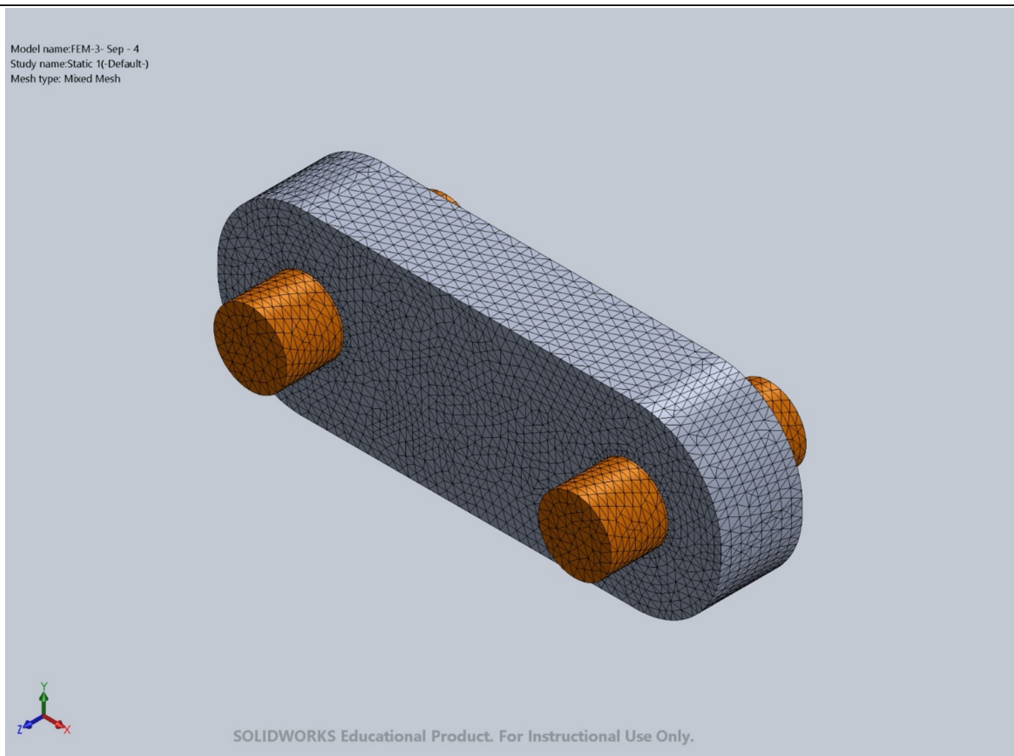	
Mesh information:	Mesh type: **Mixed mesh** Mesher used: **Curvature-based mesh**	Entities: **2 face(s)** Units: **mm**

Mesh Control:	Jacobian points: **4** Max element size: **0,123965 mm** Min element size: **0,112695 mm** Mesh Quality: **High** Total nodes: **117291** Total elements: **79631**	Size: **0,0563476** Ratio: **0,0563476**

Resultant Forces

Reaction forces:	Selection set	Units	Sum X	Sum Y	Sum Z	Resultant
	Entire model	**N**	0	0	0	1e-33
	Incorrect values due to use of rigid bodies in simulation. The force is applied on one of the rigid bodies.					

Study Results

VON: von Mises Stress	Min: 0,0 N/mm^2 (MPa) Node: 113720	Max: **135,1** N/mm^2 (MPa) Node: 27085
Picture(s)	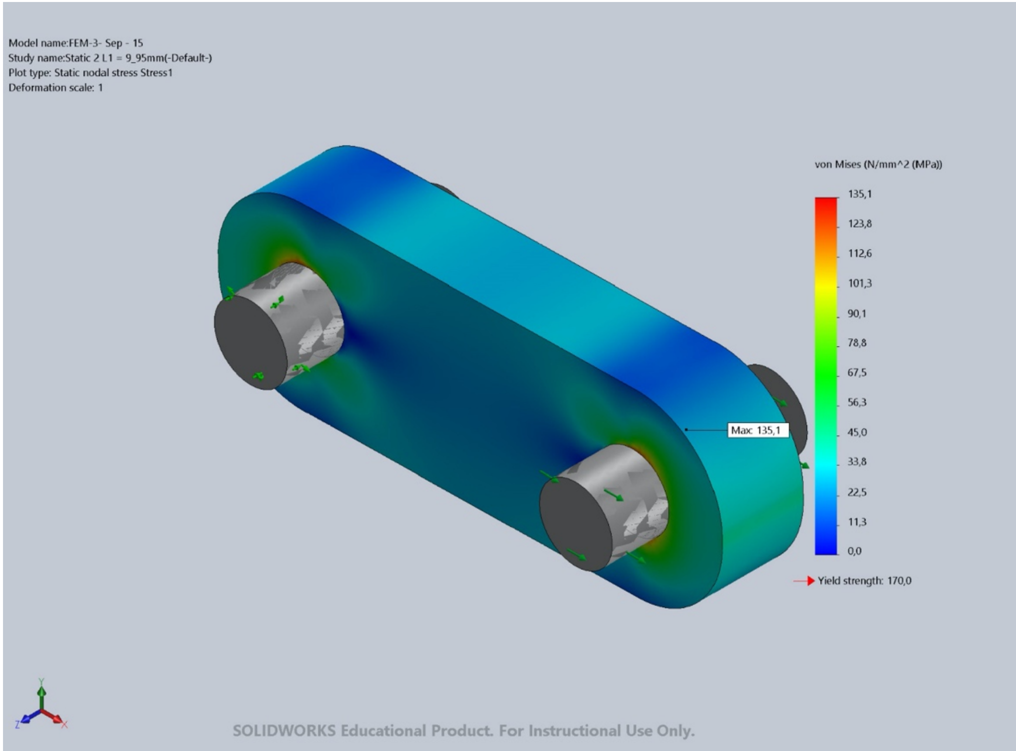	
Discussion:	The highest stress value is just below yield strength. These stresses are discussed below.	
URES: Resultant Displacement	Min: 3,969e-11 mm Node: 115856	Max: 8,482e-02 mm Node: 16

Picture(s)	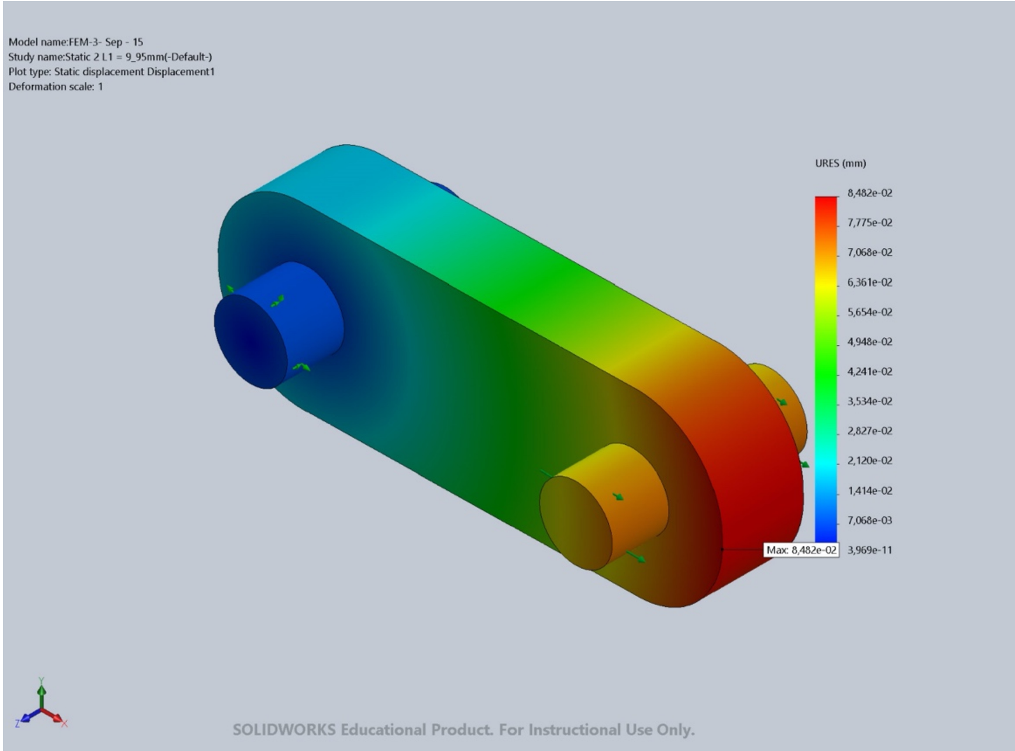	
Discussion:	Max displacement is acceptable.	
ESTRN: Equivalent Strain	Min: 0,000e+00 Element: 77848	Max: 5,370e-04 Element: 9519
Picture(s)	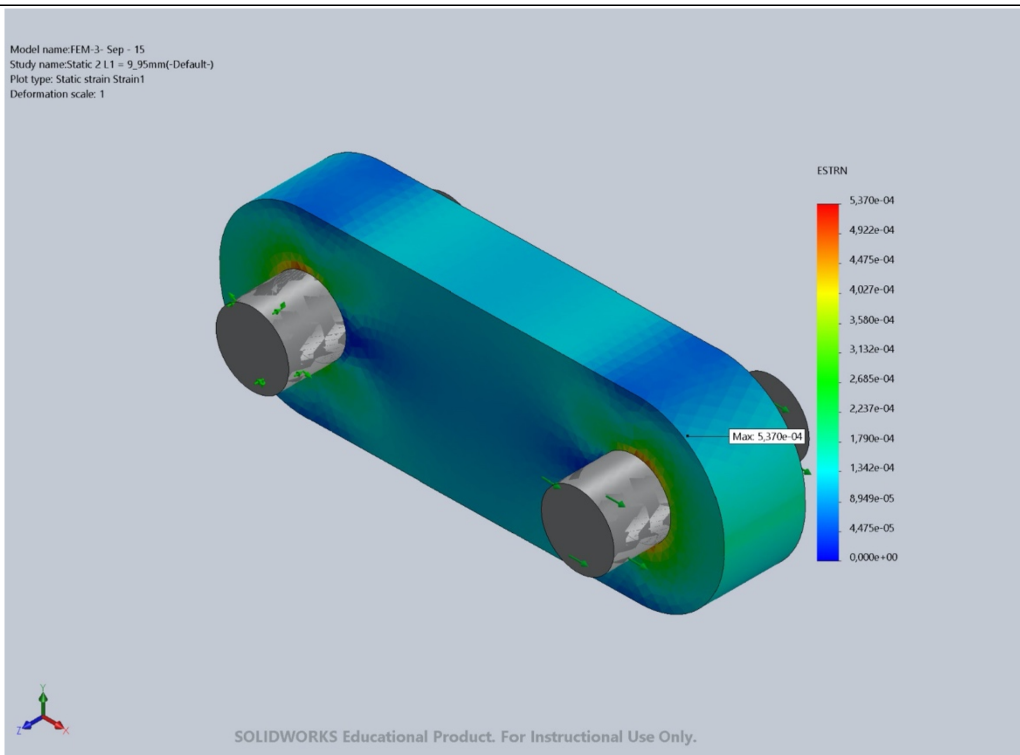	
Discussion:	Strain is acceptable. Could indicate that material does not yield.	
Factor of Safety	Min: 1,26 Node: 27085	Max: 110,12 Node: 4675

<table>
<tr><td>Picture(s)</td><td>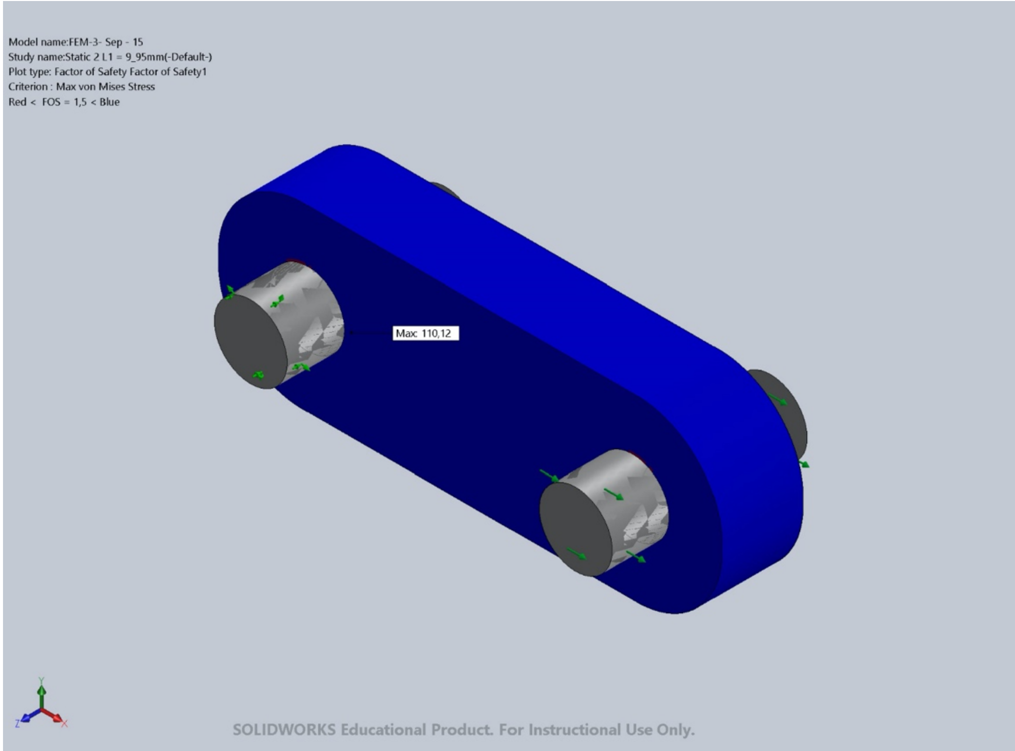
</td></tr>
<tr><td>Discussion:</td><td>Red areas: FoS <1.5. The factor of safety is below 1.5 near the high stress areas.</td></tr>
<tr><td></td><td></td></tr>
<tr><td>Additional information</td><td>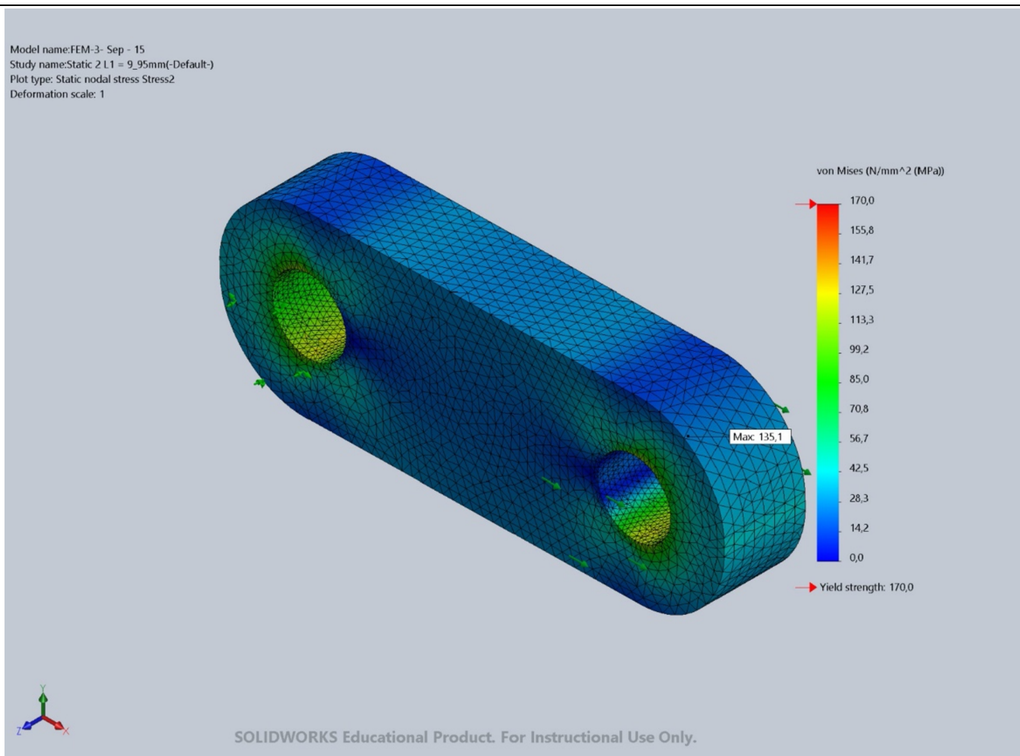
</td></tr>
<tr><td>Discussion:</td><td>This figure illustrates the elements that show high stress. Red coloured indicate stresses near yield strength, which is 170 MPa. Higher stresses occur on the surface of the first layer of elements near the hinge holes. However, the stresses in these areas are well below yield strength and show a safety factor just above 1.5.</td></tr>
<tr><td></td><td></td></tr>
</table>

Additional information	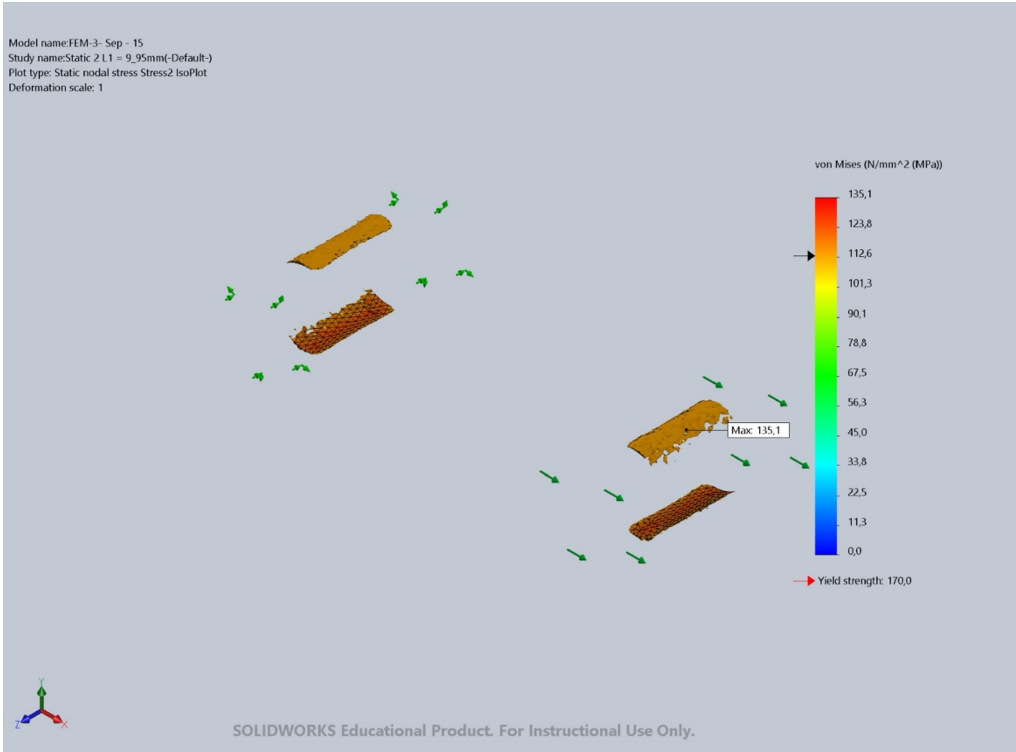
Discussion:	ISO clipping plot shows stress area >113 MPa. These are the areas where the safety factor is below 1.5.

Study Conclusion

Conclusion:	**Disregarding the stress concentrations, the Connector component appears to be strong enough to withstand the maximum applied tensile forces easily. This component is unlikely to cause problems with the maximum tensile force of 55 N applied. Fatigue problems are unlikely to occur since the safety factor of 1.5 is achieved throughout most of the component.**

FEM - 4

Simulation 4

Title:	**FEM-4 | NiTiCon**
Author:	Philip de Haes
Details:	Component No: **6** Part-file name: PH_4005_v8 – NiTiCon CAD-file name: FEM-4 - Sep – 15 Study name: Static 3 L1 = 9_95 mm Date: 15-09-2020
Summary:	The NiTiCon component is unlikely to cause problems with the maximum tensile force of 50 N applied. Fatigue problems are unlikely to occur since the safety factor of 1.5 is achieved throughout most of the component.
Assumptions:	The NiTiCon component connects the Nitinol core with the tip opening / closing mechanism. It is connected to the Connector component, forming a hinge. A rigid hinge axis constraint with a 'fixed hinge' is placed at this location. The force is attached to the face where normally the Nitinol core is bonded with the NiTiCon component. A force of 50N is applied based on previous calculations.
Study details:	Analysis type: Static Mesh type: Mixed Mesh Solver type: FFEPlus (Solidworks default) Large displacement: off
	Length/Displacement: mm Temperature: Celsius Angular velocity: Rad/sec Pressure/Stress: MPa

Model Information

Model:	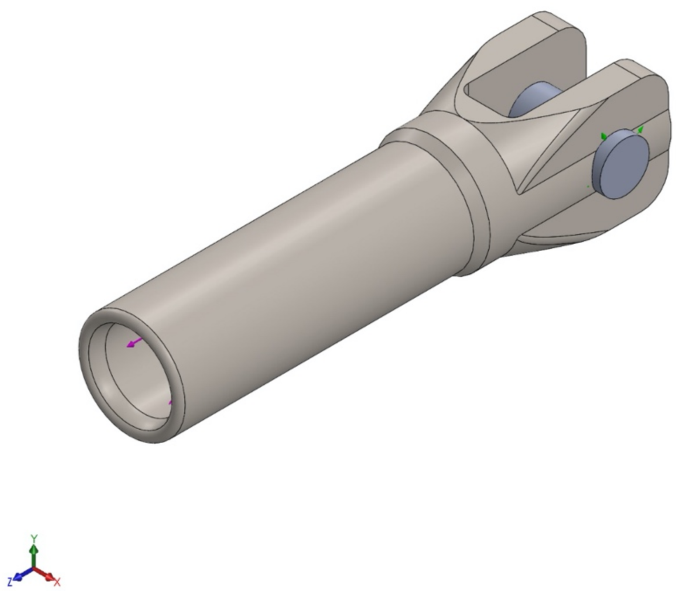

Solid bodies properties:	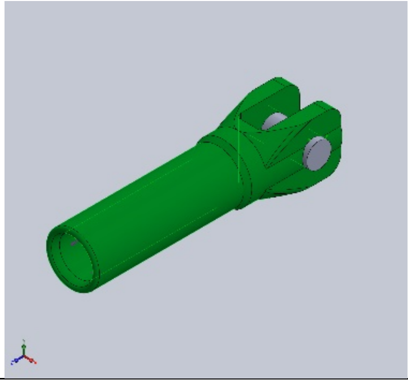	Mass: **0,000125506 kg** Volume: **1,56353e-08 m^3** Density: **8.027,1 kg/m^3** Weight: **0,00122996 N**
Material Properties:	Name: **AISI Type 316L stainless steel** Model type: **Linear Elastic Isotropic** Default failure criterion: **Max von Mises Stress** Yield strength: **170 N/mm^2** Tensile strength: **485 N/mm^2** Elastic modulus: **200.000 N/mm^2** Poisson's ratio: **0,265** Mass density: **8,027 g/cm^3** Shear modulus: **82.000 N/mm^2** Thermal expansion coefficient: **1,65e-05 /Kelvin**	

Loads and Fixtures

Fixture:	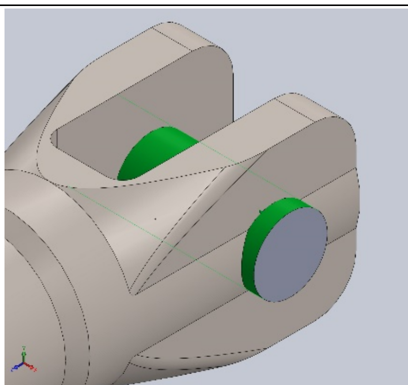	Entities: **1 face(s)** Type: **Fixed Hinge**

Resultant forces:	Components	X	Y	Z	Resultant
	Reaction Force (N)	**0**	**0**	**0**	**1e-33**
	Reaction Moment (N*m)	**0**	**0**	**0**	**1e-33**

Load:	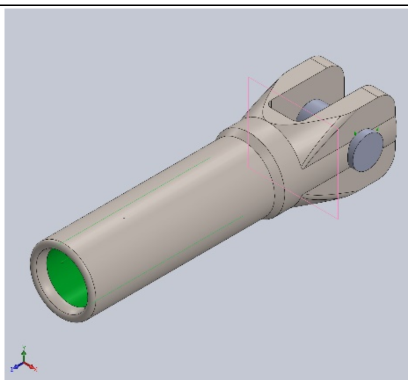	Entities: **1 face(s), 1 plane(s)** Reference: **Front Plane** Type: **Apply force** Values: **---; ---; 50 N** Moments: **---; ---; --- N.m** *This component is bonded with a Nitinol core contact the green surface (see figure on the left), similarly to where the force is attached.*

Contact information

Contact set 1:	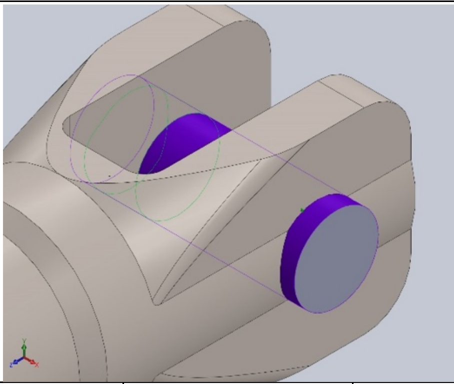			Type: **No Penetration contact pair** Entities: **2 face(s)** Advanced: **Node to surface**	
Contact/Friction force:	Components	X	Y	Z	Resultant
	Contact Force (N)	**-0,0064517**	**0,0012558**	**25,001**	**25,001**
Contact set 2:	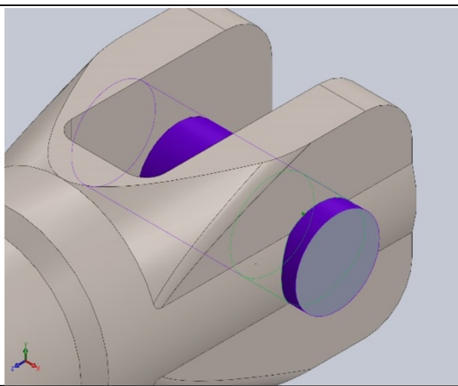			Type: **No Penetration contact pair** Entities: **2 face(s)** Advanced: **Node to surface**	
Contact/Friction force:	Components	X	Y	Z	Resultant
	Contact Force (N)	**0,0064517**	**-0,0010175**	**24,999**	**24,999**

Mesh Details

Mesh:	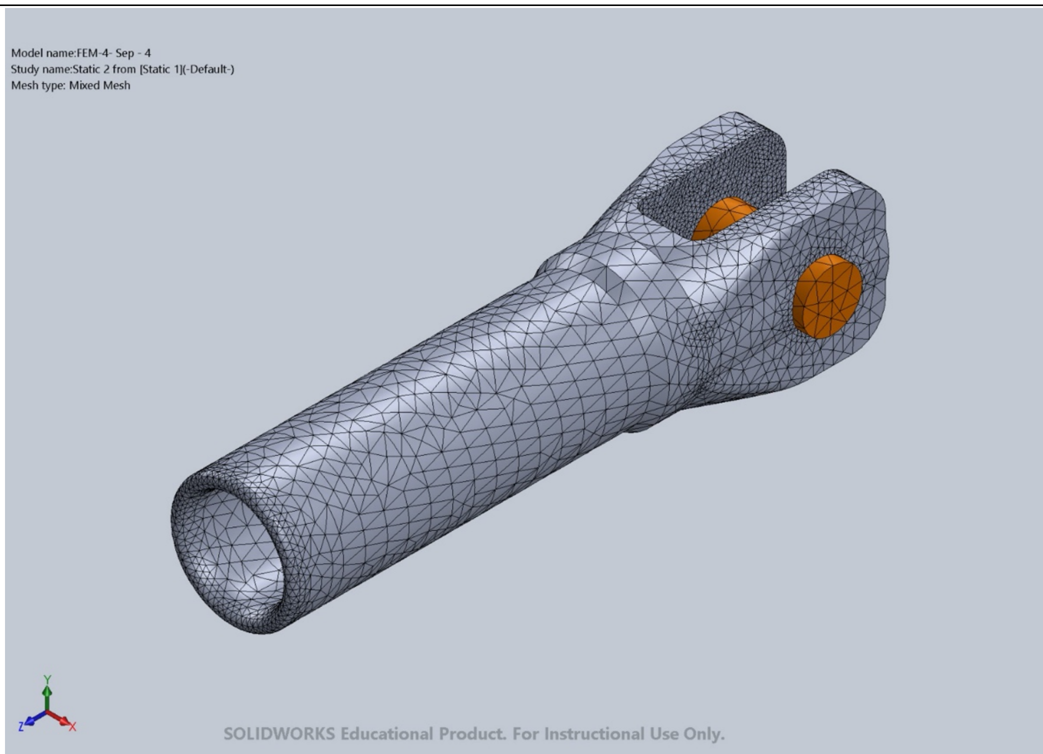

Mesh information: **Mesh Control:**	Mesh type: **Mixed mesh** Mesher used: **Curvature-based mesh** Jacobian points: **4** Max element size: **0,255602 mm** Min element size: **0,0511204 mm** Mesh Quality: **High** Total nodes: **84748** Total elements: **54599**	Entities: **4 face(s)** Units: **mm** Size: **0,0639003** Ratio: **0,0639003**

Resultant Forces

Reaction forces:	Selection set	Units	Sum X	Sum Y	Sum Z	Resultant
	Entire model	**N**	**0**	**0**	**0**	**1e-33**

Study Results

VON: von Mises Stress	Min: 0,0 N/mm^2 (MPa) Node: 84299	Max: 134.6 N/mm^2 (MPa) Node: 12717
Picture(s)	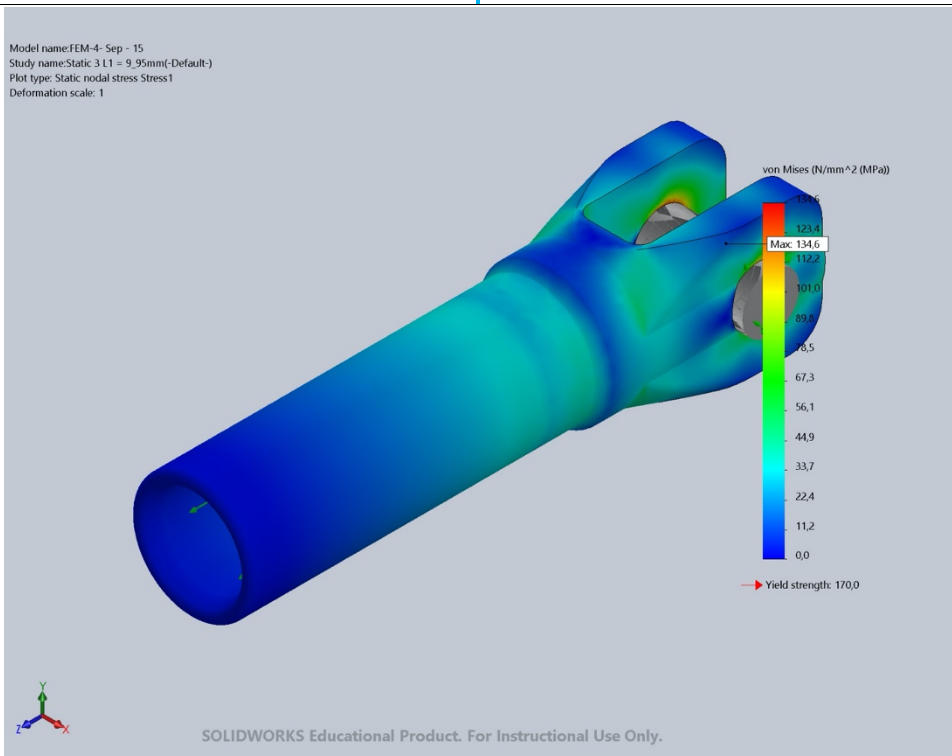	
Discussion:		
URES: Resultant Displacement	Min: 2,439e-11 mm Node: 84400	Max: 2,534e-03 mm Node: 5627

<table>
<tr><td>Picture(s)</td><td colspan="2">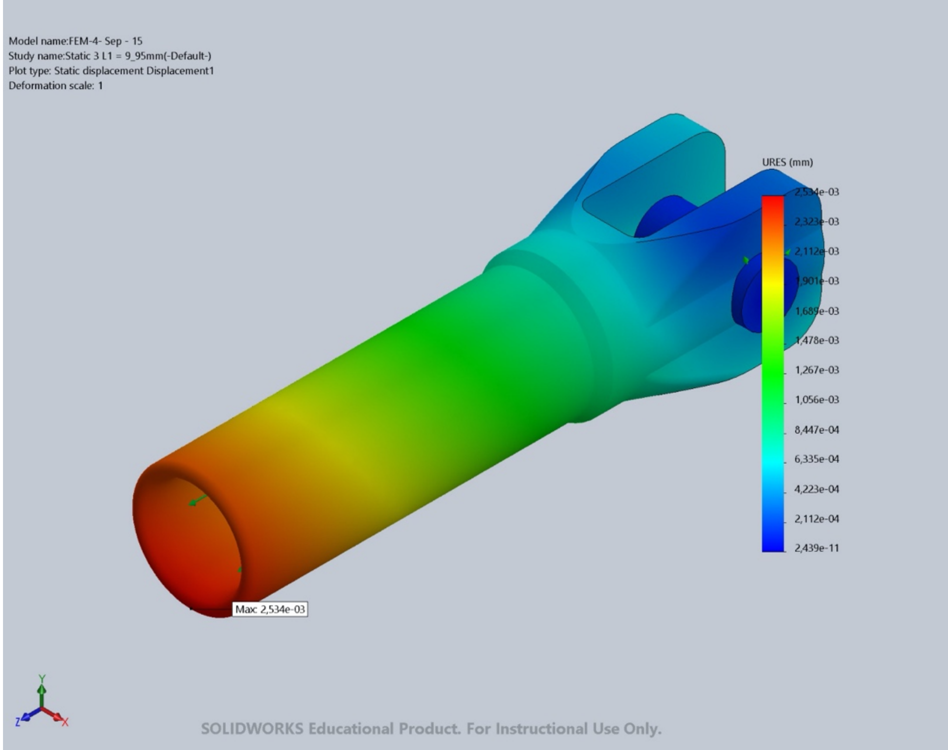
</td></tr>
<tr><td>Discussion:</td><td colspan="2">Displacements are acceptable.</td></tr>
<tr><td>ESTRN:
Equivalent Strain</td><td>Min: 0,000e+00
Element: 54376</td><td>Max: 5,397e-04
Element: 14529</td></tr>
<tr><td>Picture(s)</td><td colspan="2">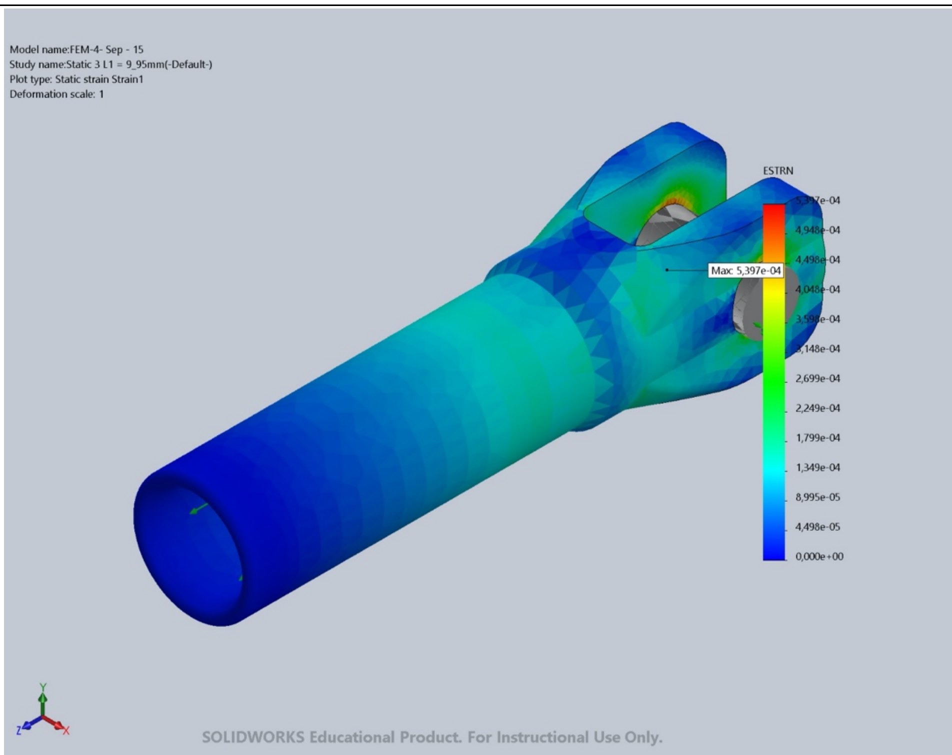
</td></tr>
<tr><td>Discussion:</td><td colspan="2">Strain is acceptable and could indicate that the material doesn't yield.</td></tr>
<tr><td>Factor of Safety</td><td>Min: 1,26
Node: 12717</td><td>Max: 325,20
Node: 6034</td></tr>
</table>

<table>
<tr><td>Picture(s)</td><td>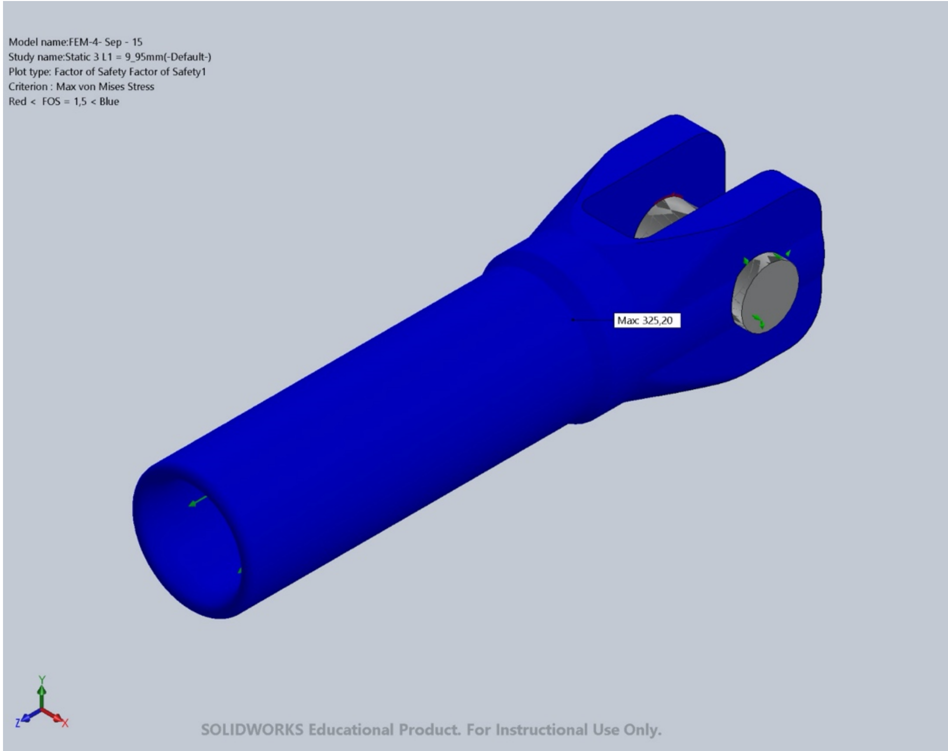
</td></tr>
<tr><td>Discussion:</td><td>Red areas: FoS <1.5. Similarly to the stress plot, the red areas indicate high stresses.</td></tr>
<tr><td>Additional information</td><td>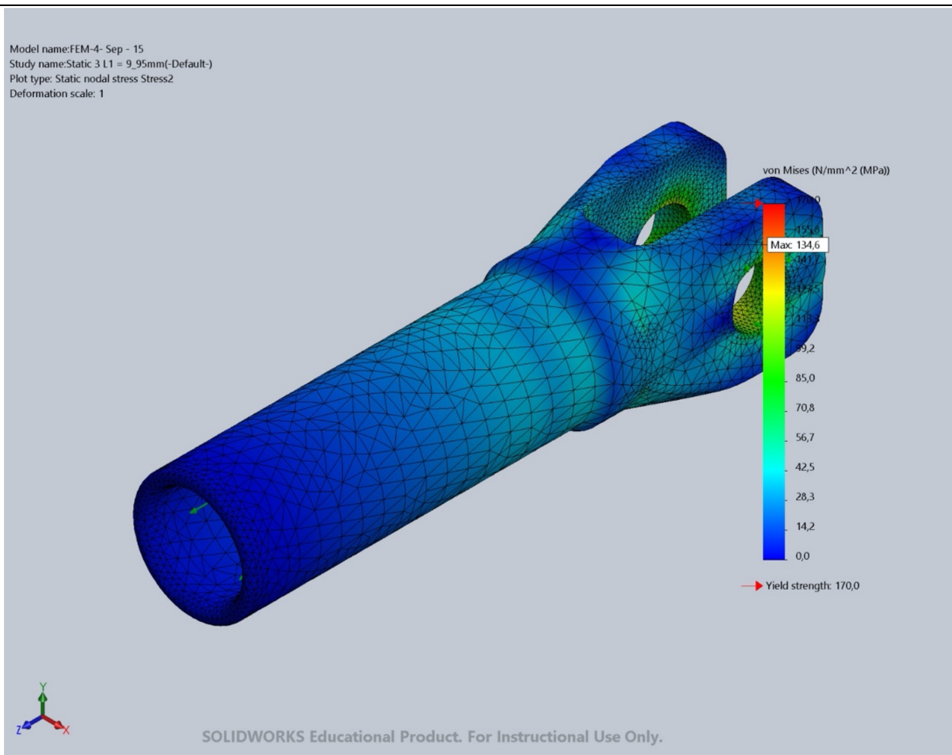
</td></tr>
<tr><td>Discussion:</td><td>This figure illustrates the elements that show high stress. Red coloured indicate stresses near yield strength, which is 170 MPa. No red coloured elements appeared. The maximum stress 134.6 MPa well below 170 MPa.</td></tr>
</table>

Additional information	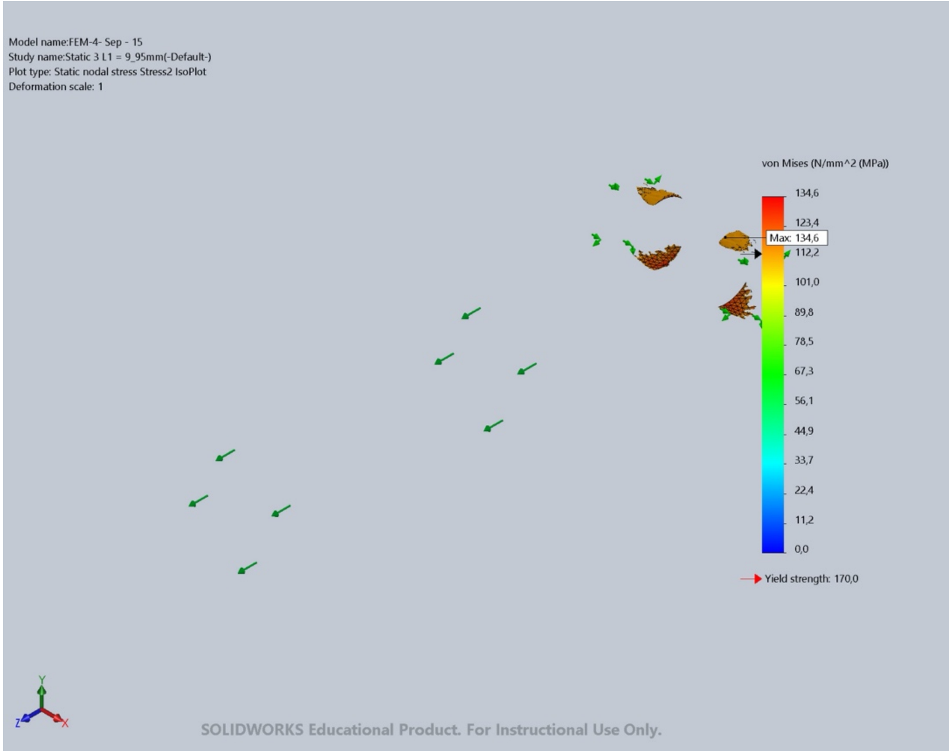
Discussion:	ISO clipping plot shows stress areas (elements) with a safety factor below 1.5, thus stresses above 113 MPa. This figure shows that the stress does not radiate deeper into the material instead only the a few elements near the surface are affected.

Study Conclusion

Conclusion:	Based on the above results, this component is unlikely to cause problems with the maximum tensile force of 50N applied. Fatigue problems are unlikely to occur since the safety factor of 1.5 is achieved throughout most of the component.